ELSEVIER

Journal of Marine Systems 31 (2001) 99–135

JOURNAL OF MARINE SYSTEMS

www.elsevier.com/locate/jmarsys

Mixing in the Bosphorus Strait and the Black Sea continental shelf: observations and a model of the dense water outflow

Emin Özsoy [a,*], Daniela Di Iorio [b], Michael C. Gregg [c], Jan O. Backhaus [d]

[a] *Institute of Marine Sciences, Middle East Technical University, P.O. Box 28, Erdemli, Icel, 33731 Turkey*
[b] *Department of Marine Sciences, University of Georgia, Marine Sciences Building, Athens, GA, 30602 USA*
[c] *Applied Physics Laboratory, College of Ocean and Fishery Sciences, University of Washington, 1013 NE 40th St., Seattle, WA, 98105-6698 USA*
[d] *Institut für Meereskunde an der Universität Hamburg, Troplowitzstrasse 7, D-22529, Hamburg, Germany*

Received 17 January 2000; accepted 28 June 2001

Abstract

Counterflowing waters of the Black Sea and Mediterranean Sea are mixed by turbulent entrainment processes along their course through the Turkish Straits. In the Bosphorus Strait, the entrainment into the upper layer from below is abruptly increased when the flow is accelerated in the narrower southern reach, where the flow passes through a contraction. In contrast, the lower layer salinity decreases towards the north first by gradual entrainment within the Strait and later at an increased rate in the wide continental shelf region upon exit into the Black Sea. After passing over the sill located north of the Strait, the flow on the continental shelf proceeds in the form of a gravity current following the local slopes. The topography of the shelf region, assembled from various sources of high-resolution surveys and maps, is reminiscent of a river delta. The water properties and thickness of the Mediterranean plume is modified by turbulent entrainment, shelf currents, stratification, bottom friction and slope. The flow first spreads out on the mid-shelf slope, follows the delta features to reach the shelf edge and, finally, cascades down the steep continental slope. Horizontal spreading by convective instabilities and eastward propagation of anomalous properties along the continental slope are characteristic features of the deeper region adjacent to the shelf. The behaviour of the density current is revealed by results obtained from a reduced gravity model, suggesting that the slope and fine-scale features of the bottom topography are crucial elements in determining plume behaviour. The model results are found to be robust to environmental changes and in good correspondence with observed flow features, especially when the topography with realistic fine scales and slope are adequately represented.

Keywords: Straits; Outflow; Friction; Entrainment; Continental shelf; Black Sea; Bosphorus; Mediterranean

1. Introduction

The Turkish Straits System (TSS), consisting of the Bosphorus and Dardanelles Straits and the Sea of Marmara, provides the only mechanism of communication between the Black and the Mediterranean Seas. The TSS is located in a region with demonstrated sensitivity to climatic changes and contrasts

* Corresponding author. Tel.: +90-324-521-2406; fax: +90-324-521-2327.
E-mail addresses: ozsoy@ims.metu.edu.tr (E. Özsoy), daniela@arches.uga.edu (D. Di Iorio), gregg@apl.washington.edu (M.C. Gregg), backhaus@dkrz.de (J.O. Backhaus).

0924-7963/01/$ - see front matter
PII: S0924-7963(01)00049-5

(Özsoy, 1999), and it is also capable of driving environmental changes in the adjacent basins disproportionate to its relative size. Recently recovered evidence suggesting abrupt flooding of the Black Sea about 7500 years BP (Ryan and Pitman, 1998) attests to the possible level of climatic impacts of the Straits. Among the two Straits, the Bosphorus plays a predominant role, determining local transport (Özsoy et al., 1995b) and exchange (e.g. Ünlüata et al., 1990).

In the 17th century, Count Marsigli was the first one to make scientific observations in the Bosphorus and to perform insightful experiments (Marsigli, 1681) establishing the existence of counter-currents underneath the surface currents, a fact well known by local fishermen (Deacon, 1971), but occasionally obscured by incomplete observations, only to be recovered later by additional measurements (Deacon, 1971; Ünlüata et al., 1990). Modern observations have revealed persistent exchange flows, despite short-term blocking periods (Latif et al., 1991; Özsoy et al., 1998a).

The geometrical elements (Oğuz et al., 1990; Ünlüata et al., 1990; Özsoy et al., 1998a) of the Bosphorus are ideally situated to support 'maximal exchange' (Farmer and Armi, 1986), a special regime for hydraulically controlled strait flows. At the contraction (the narrowest section) at about one-third the length of the Strait from the southern end (Figs. 1 and 2a), both layers are expected to pass through a flow transition, where F_1 and F_2, the individual Froude numbers for each layer, are increased, such that the composite Froude number $G^2 = F_1^2 + F_2^2$ approaches the critical value $G^2 = 1$. The other control section with $G^2 \simeq F_2^2 = 1$ occurs at the sill located about 5 km north of the Strait, where the faster lower layer flow confined in the bottom canyon (Fig. 2a) is the main participant in the sill hydraulic control. Rapid along-strait variations of geometry, sharp stratification and nonlinear controls are important elements of the dynamics of the Bosphorus, resulting in temporary blocking of the exchange flows and time dependence on daily to interannual time scales, driven by barometric pressure, wind set up, sea level and water budgets (Ünlüata et al., 1990; Oğuz et al., 1990; Özsoy et al., 1995a, 1996, 1998a; Ducet et al., 1999; Gregg and Özsoy, 1999; Gregg et al., 1999; Gregg and Özsoy, 2001).

In Fig. 1, main flow features of the Bosphorus Strait are visualized by making use of Synthetic Aperture Radar (SAR) data. The southward-flowing surface jet issuing into the Marmara Sea from the Bosphorus impinges on the south coast, exciting an internal wave packet visible on the surface. Surface roughness changes resulting from currents are sensitively detected by the SAR. A conspicuous curved feature extending north from the Bosphorus joined with a wider shadow further offshore in the Black Sea coincides well with the location of the submerged Mediterranean outflow investigated in the present paper. This correspondence is striking because shallow bottom topographic features are known to be reflected in SAR data, depending on their effects on the currents (Wensink and Campbell, 1997).

The seawater properties in the counter-flowing layers of the Turkish Straits System are continuously modified by two-way turbulent entrainment, especially inside the Bosphorus and Dardanelles Straits, past the suggested hydraulic controls in the southern and northern extremities of the strait, and when the flow exits into adjacent seas (e.g. Ünlüata et al., 1990).

The Mediterranean water outflowing to the Black Sea continues to be modified by turbulent entrainment in the shelf region. Topography plays an important role in the exit region of the Bosphorus Strait, where the warm, saline Mediterranean water enters the Black Sea and, after overflowing a sill, spreads as a thin plume on the continental shelf (Yüce, 1990; Latif et al., 1991; Di Iorio and Yüce, 1998; Di Iorio et al., 1999; Gregg et al., 1999). The ratio of the entrainment flux over the shelf to the input from the Bosphorus has been estimated to be 3–6 (Özsoy et al., 1993). The dense water sinking at the continental slope drives convection with intermittent filaments of intrusive waters at depths of 100–500 m to the east of the source in the entire southwestern Black Sea, identified with anomalous temperature, particle and nutrient concentrations (Özsoy and Beşiktepe, 1995; Özsoy et al., 1993). An important consequence of the boundary mixing created by the plume and its cascade at the shelf break is the active ventilation of the anoxic waters of the Black Sea interior at intermediate depth (Özsoy and Ünlüata, 1997, 1998; Özsoy et al., 1993), as confirmed by tracer measure-

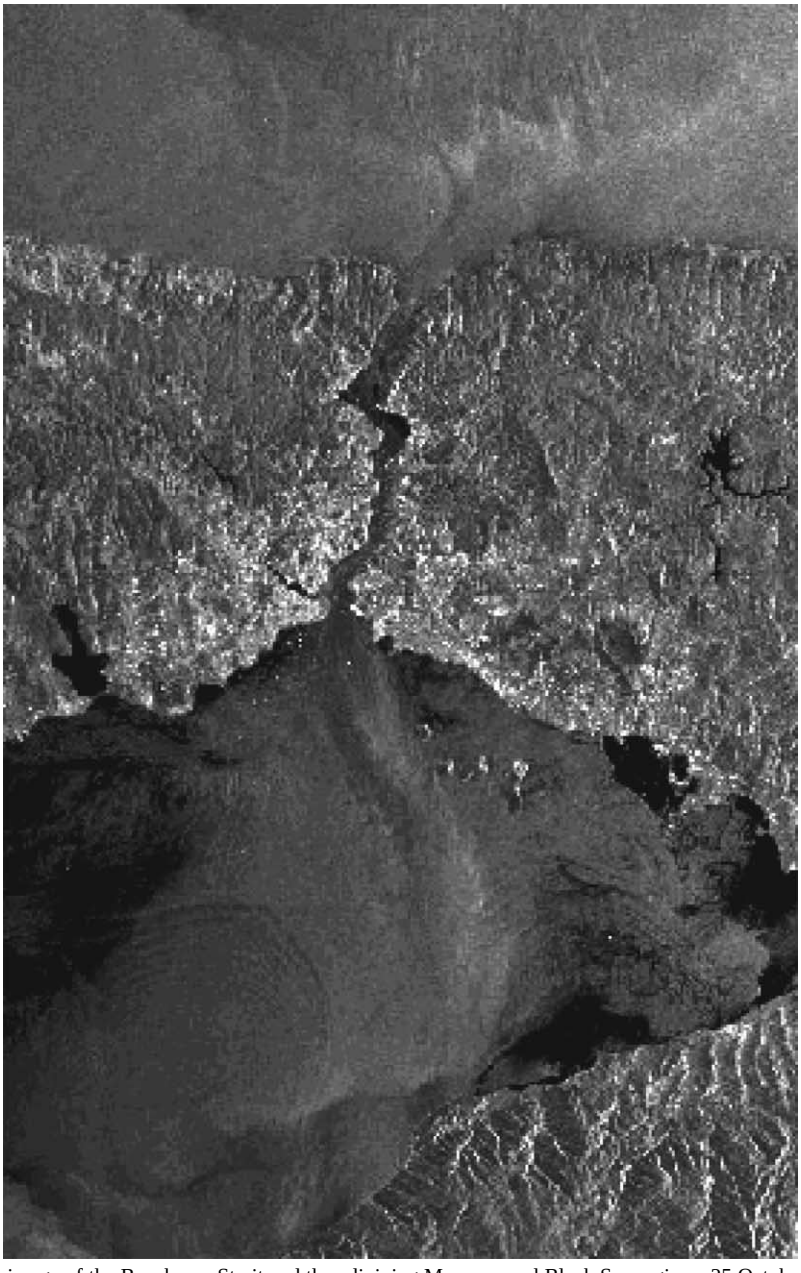

Fig. 1. ERS-1 SAR image of the Bosphorus Strait and the adjoining Marmara and Black Sea regions, 25 October 1995, 8:49 GMT.

ments (Rank et al., 1998; Özsoy et al., in press) as well as through plume parameterization in 3-D models (Staneva et al., 1999).

For an extensive assessment of gravity currents, the reader is referred to Griffiths (1986). A variety of oceanic examples similar to the present case can be found in many places, especially at slopes near sills of semienclosed seas, and have been investigated in different contexts, using analytical tools and models of varying complexity, e.g. the Denmark Strait

(Jungclaus, 1994; Jungclaus and Backhaus, 1994) and the Mediterranean effluent in the Atlantic Ocean (Baringer, 1994). Experimental and theoretical studies (Shapiro and Hill, 1997; Shapiro and Zatsepin, 1997) indicate different regimes of behaviour depending on time, distance from source and the para-

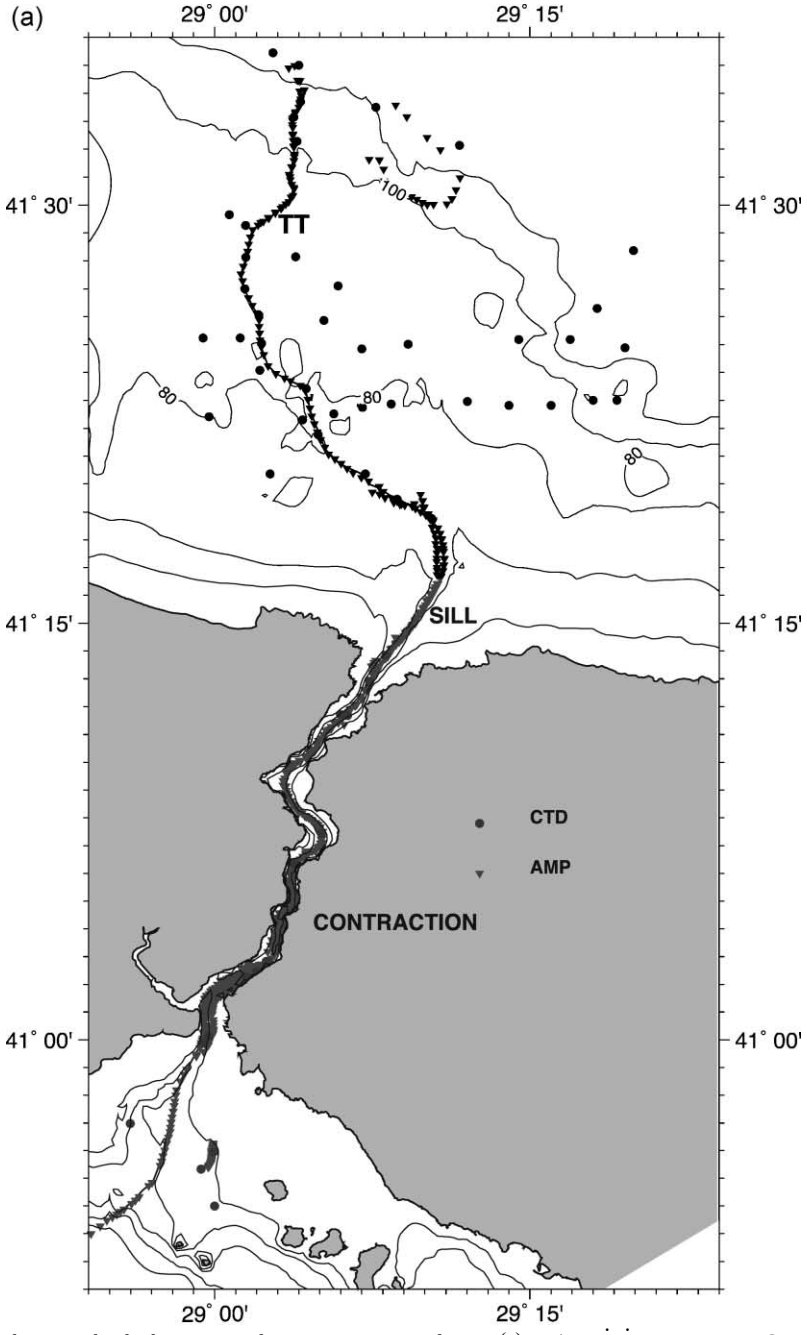

Fig. 2. Location map showing the bathymetry and station positions during (a) R/V BİLİM surveys in September 1994, (b) R/V ALLIANCE surveys in June 1996. The large circles mark stations where intrusive layering was observed in 1996, corresponding to temperature profiles displayed in Fig. 5.

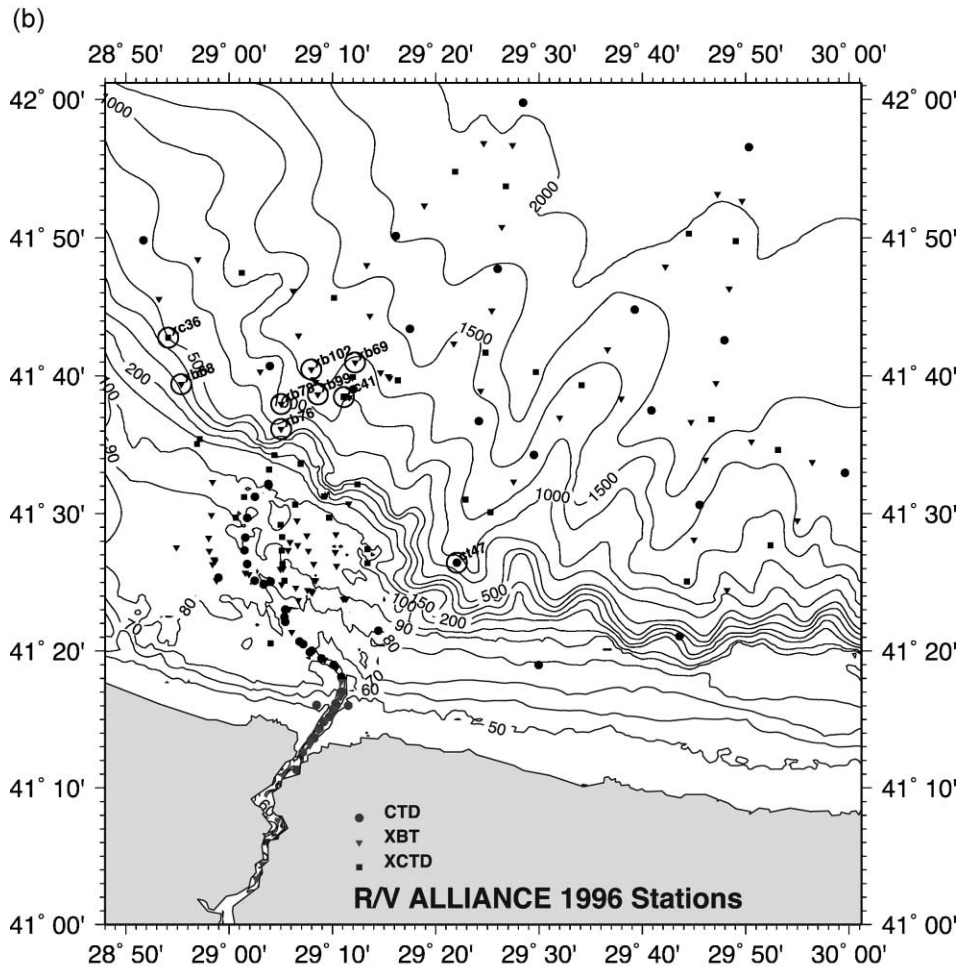

Fig. 2 (*continued*).

metric setting. An important side effect of dense water outflows is the generation of eddies in the ambient fluid by the bottom plume (Lane-Serff and Baines, 1998; Zatsepin et al., 1998; Etling et al., 2000). In Black Sea context, lateral inputs of buoyancy (Stanev, 1990), as well as changes in continental shelf and slope topography (Özsoy et al., 1993; Sur et al., 1994; Sur et al., 1996), have been suggested as possible mechanisms to excite eddies and meandering jets along the coast, largely overlooking the above mechanism.

In the following sections, we study the mixing between counter-flowing currents along the Bosphorus Strait, as well as in the outflow of Mediterranean water into the Black Sea, based on extensive data collected at sea and the results of a reduced gravity model. The model is based on primitive equations, incorporating the effects of real bottom topography, property changes resulting from entrainment, nonlinear effects of advection and of the fluid interface, lateral and bottom friction (Appendix A). The same model has been used by Simeonov et al. (1997) for exploratory work, and later by Stanev et al. (2001) for parametric studies. Our interest in the present paper is to create and discuss a set of simulations best suited for the Black Sea conditions with guid-

ance obtained from a combined set of modern observations.

In the next section, we describe the set of measurements used in the subsequent analyses. In Section 3, we review the mixing processes in the Bosphorus Strait and its Black Sea exit, while in Section 4, we reconstruct the bottom topography of the continental shelf from recent sources of high-resolution data to be able to adequately describe the topographic slopes in the numerical modelling of the dense flow. In Section 5, we describe the results obtained from modelling together with interpretations based on observations. In Section 6, we provide a discussion of the model sensitivity to included parameters and to processes not accounted for at present. Finally, in Section 7, we provide general conclusions and a brief discussion of implications for other fields.

2. The measurements

Hydrography and currents on the continental shelf and slope regions adjacent to the Bosphorus exit in the Black Sea were investigated during numerous cruises of the R/V BİLİM of the IMS-METU from 1986 to the present (references cited above).

In September 1994, scientists from the University of Washington (APL/UW) and IMS-METU carried out collaborative studies on board the R/V BİLİM making intensive measurements using ADCP, CTD, Advanced Microstructure Profiler (AMP), current meters, sea-level instruments and acoustic backscatter imaging of the physical features (Gregg and Özsoy, 1999; Gregg and Özsoy, 2001; Gregg et al., 1999). Numerous bursts of AMP stations, as well as CTD stations shown in Fig. 2a, yielded data with high horizontal resolution along the strait.

Collaborative studies of the Bosphorus outflow to the Black Sea were made on board the NATO/SACLANT ship R/V ALLIANCE in 1996 with measurements of temperature and salinity from CTD, XBT and XCTD sensors (Fig. 2b), currents from fixed current meters and ADCP profilers, sea level at fixed stations, as well as acoustical backscatter imaging, and acoustical scintillography measurements of currents and turbulent dissipation. In addition, a high-resolution depth survey was made with the SWATH instrument (Di Iorio et al., 1999).

3. Mixing in the Bosphorus and the Black Sea exit

Because the mean properties for flows in each direction varied along the strait, local definitions rather than fixed values were needed for limiting properties of layers. We first calculated typical surface and bottom salinity values, S_s and S_b, respectively, by averaging salinity within 5 m of the surface and bottom, this depth interval being selected for detection purposes, countering problems with missing profile data or disturbances near the surface and the bottom. Then, we defined $S_1 = S_s + 0.2(S_b - S_s)$ and $S_2 = S_b - 0.2(S_b - S_s)$ as the local transition values of the upper and lower layers, respectively (assuming each layer contains 20% of the salinity variation in the two-layer stratified profile), enabling calculation of the thickness and average properties of layers displayed in (Figs. 3, 4, 6 and 11). An interfacial layer of ~ 10 m thickness, accounting for the remaining 60% of the salinity range, thus occurred between the upper and lower layers.

In Fig. 3, a thin interfacial layer extends between the two principal control sections of the Bosphorus, i.e. the contraction and sill. In contrast, the interface becomes thicker in two areas as a result of increased mixing: the thickening of the interface, with a remarkable simultaneous increase of upper layer salinity from 18 to 23 occurs south of the contraction (at 11 km in Figs. 3 and 4). The interface thickness is also increased in the Black Sea, north of the sill. Both the interface and the lower layer finally become much thinner when dense water emerges onto the flat-shelf region after leaving the deep bottom canyon leading north from the Bosphorus.

Salinity is a conservative tracer, and the horizontal gradient of its layer average is, therefore, a good indicator of the rate of entrainment. The continuous decrease of lower layer salinity from the Marmara Sea to the Black Sea is proportional to the rate of entrainment of low salinity waters from above. The horizontal gradient of salinity becomes smaller in the northern Bosphorus where the increased stability of the interface appears to limit entrainment. Entrainment is greatly increased past the northern sill (5 km

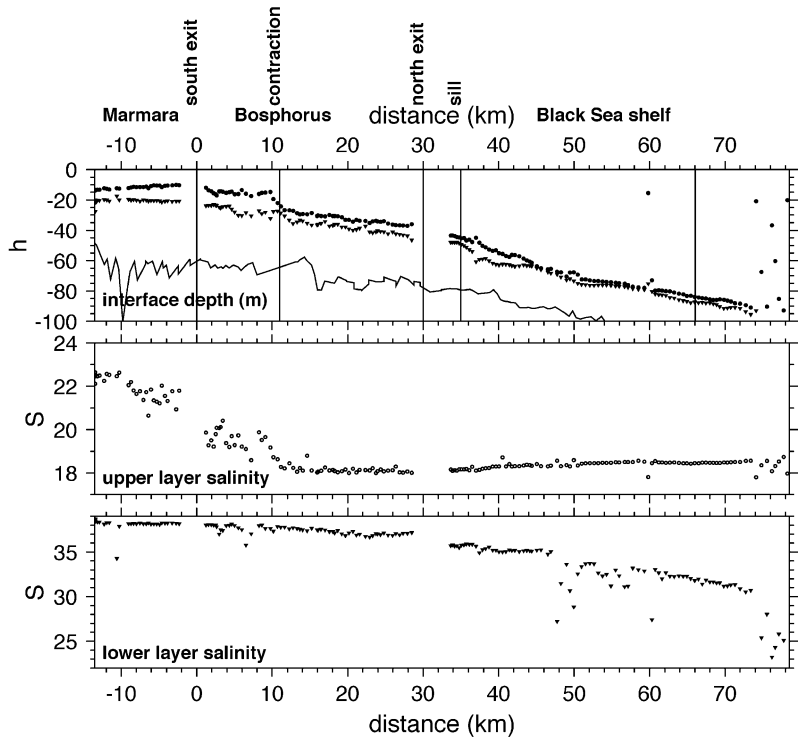

Fig. 3. Variation of the upper and lower layer depths, and average salinity of the upper and lower layers, for the composite section of AMP drops along transect TT (Fig. 2a) across the Bosphorus Strait (179 profiles) during 13–19 September 1994.

from the Bosphorus exit), and a further increase occurs when the flow exits the canyon and spreads on the flat-shelf region (20 km from the northern end). Finally, with the increased slope at the shelf edge (55 km from the northern end), the bottom layer can only be identified with difficulty, but few data points where it could be detected show entrainment increased by an order of magnitude in comparison to the flat region. Yet, the Mediterranean effluent survives with a salinity of 31 before arriving at the shelf break and completely loses its identity shortly thereafter.

In Fig. 4, the salinity distribution across transect TT extending through the Bosphorus into the Marmara and Black Sea regions shows the full detail of the property changes. Horizontal discontinuities at certain regions, such as near the northern end of the Bosphorus, should be disregarded as separate bursts of data separated by a few days in time were combined here. In addition to the lengthwise variations in salinity, there are strong gradients at the interfacial layer approaching from the bottom and the top. Small-scale oscillations in salinity and layer thickness are revealed in Figs. 3 and 4. Inside the Bosphorus, oscillations with wavelengths less than a few kilometers are enhanced near the interface. These oscillations most likely are associated with turbulent structures. Features with somewhat larger horizontal scales in the adjacent basins could be imprints of mesoscale eddies.

The outflows during the 1994 and 1996 surveys were similar in character and, therefore, the shelf transects for 1996 are not shown. The data immediately offshore of the shelf region are instead used to show cold-water anomalies, characterizing the intrusions of modified shelf waters in Fig. 5. The most characteristic signature of the injected waters in the vicinity of the shelf and intermittently over the entire

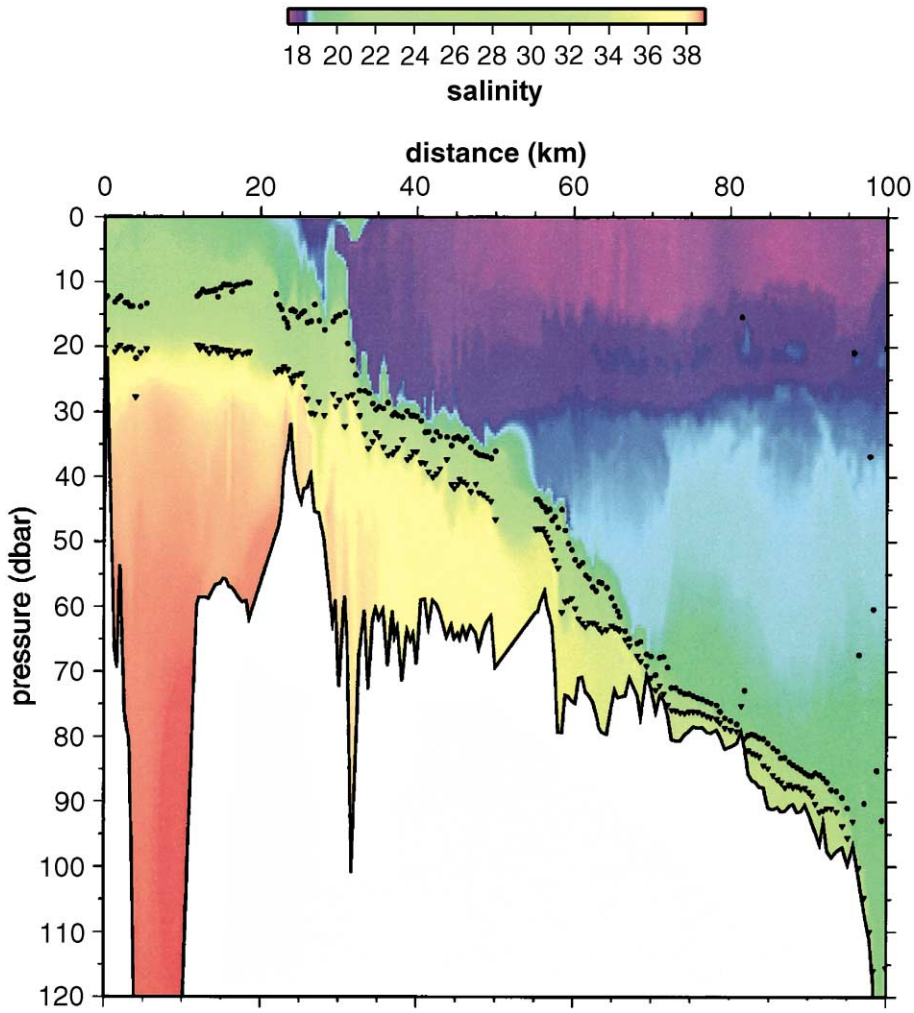

Fig. 4. Salinity section along transect TT constructed from the data of 179 AMP drops across the Bosphorus Strait during 13–19 September 1994, Fig. 2a.

southwestern Black Sea to the east of the Bosphorus are double diffusive intrusions identified with anomalous temperature, particle and nutrient concentrations in intermediate depths, ca. 100–500-m depth (Özsoy and Beşiktepe, 1995; Özsoy et al., 1993). The locations of the deep temperature profiles with anomalous distributions corresponding to the intrusions are shown by the large empty circles in the station map of Fig. 2. The rest of the profile data at the other stations are free of such features. The locations of the intrusions suggest entry of the shelf modified Mediterranean waters along a wide region north of the Bosphorus, but, especially, in the region adjacent to the shelf-edge delta (see Fig. 8) at 41°35′N 29°05′E, suggesting the role of the bottom topography in channeling the dense outflow.

The bottom layer salinity at CTD and XCTD stations of the 1994 and 1996 experiments in Fig. 6a and b reveal a region of high salinity extending from Bosphorus to the shelf edge, consistent with earlier studies (Latif et al., 1991). The only area where salinity values of up to 31–32 survive till the shelf

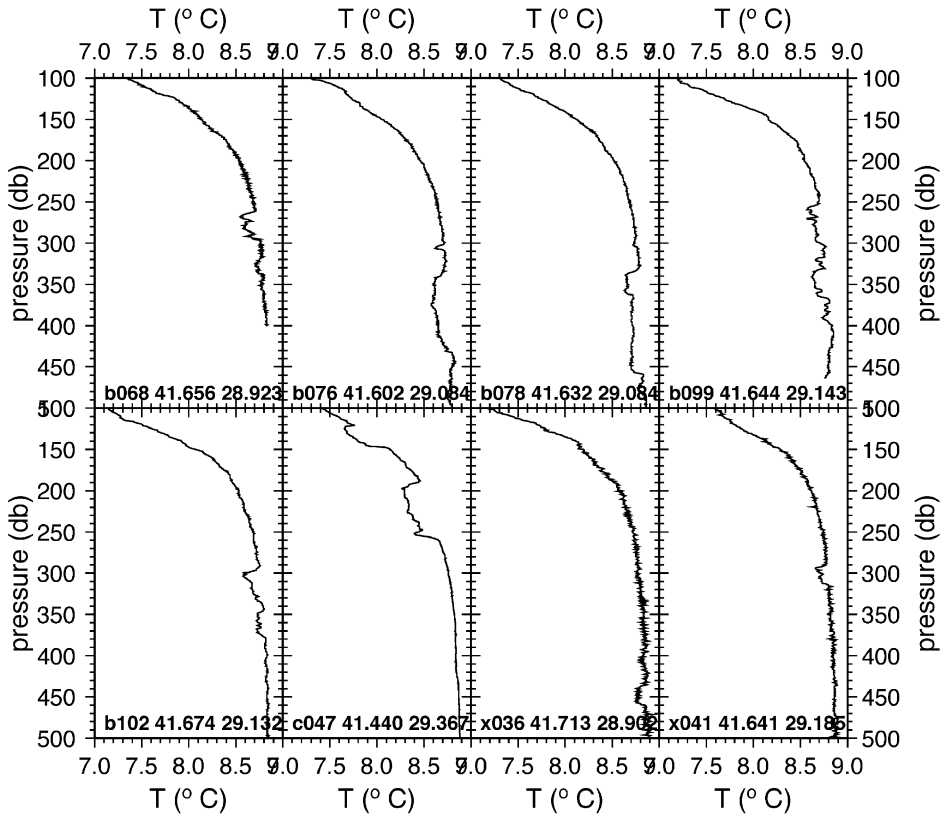

Fig. 5. Temperature profiles with intrusive layering during the 1996 experiment. The station locations are those shown with open circles in Fig. 2b.

edge (depth ≃ 100 m) is within the neighborhood of the bottom groove extending up to a distance of 45 km from the Bosphorus exit (Figs. 3 and 4). In 1994, moderately high values of salinity also occurred in the region where the bottom gently slopes down to the east of the groove, decreasing to 28.6 at the shelf break adjacent to the Bosphorus Canyon at 29°15′E 41°25′N, suggesting eastward leakage of water from the main dense water vein. Salinity measured on the continental slope is considerably smaller, with a maximum of about 28 detected at 200-m depth immediately near the shelf-edge termination of the bottom groove. No further sign of anomalous salinity survives at deeper depths. The features either suggest rapid dilution of the waters cascading on the continental slope or that they are difficult to be traced by measurements.

Turbulence measurements on the Black Sea shelf during the 1994 experiment (Gregg and Özsoy, 1999) have shown turbulent dissipation rates of $\epsilon = 10^{-5}$–10^{-3} W kg^{-1} (estimated over successive intervals of 0.5 m) within the outflow plume. Similar measurements using an acoustic scintillation system during the 1996 experiment (Di Iorio and Yüce, 1998; Di Iorio et al., 1999) have produced path-integrated dissipation rates of up to 10^{-4} W kg^{-1} within the Mediterranean water at the sill. The turbulent dissipation in the outflow plume during 1994 slightly decreased until the shelf edge, but remained active in the continental slope region, at a distance of 5 km from the shelf break, up to a depth of 200 m within the depth range covered by the measurements, with maximum values of up to 10^{-4} W kg^{-1} (Gregg and Özsoy, 1999), while the background turbulent dissi-

pation of the Black Seawaters below the surface mixed layer and above the plume was found to correspond to some of the lowest values of diapycnal diffusivity ever observed in the world ocean. It was conjectured that these values represented a background internal wave field at the time of the measurements, which was probably the only source of turbulence in the absence of wind mixing and tides (Gregg, 1998).

The 120 kHz echo-sounding images of Fig. 7b and c along transects of Fig. 7a illustrate a thin near-bottom layer of anomalous water identified with a sharp interface. The visualization by the acoustic scattering images provide confirmation of detailed structure of the dense Mediterranean water overflow along the sill, the bottom channel and across the shelf slope. The main overflow across the sill follows the bottom channel and groove in continuation until the shelf edge. Deviations from this main path and leakage across the main path into the adjoining areas are supported by the complex local topography. In the echo-sounding images, the bottom topography

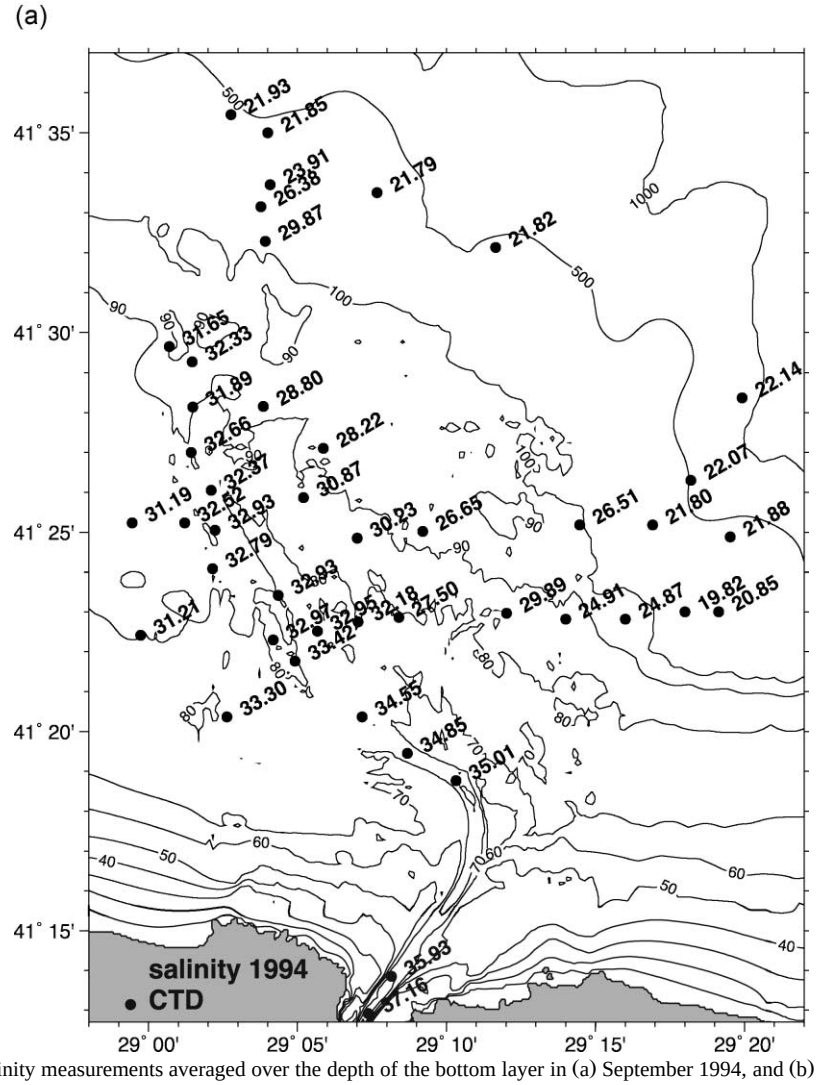

Fig. 6. Salinity measurements averaged over the depth of the bottom layer in (a) September 1994, and (b) June 1996.

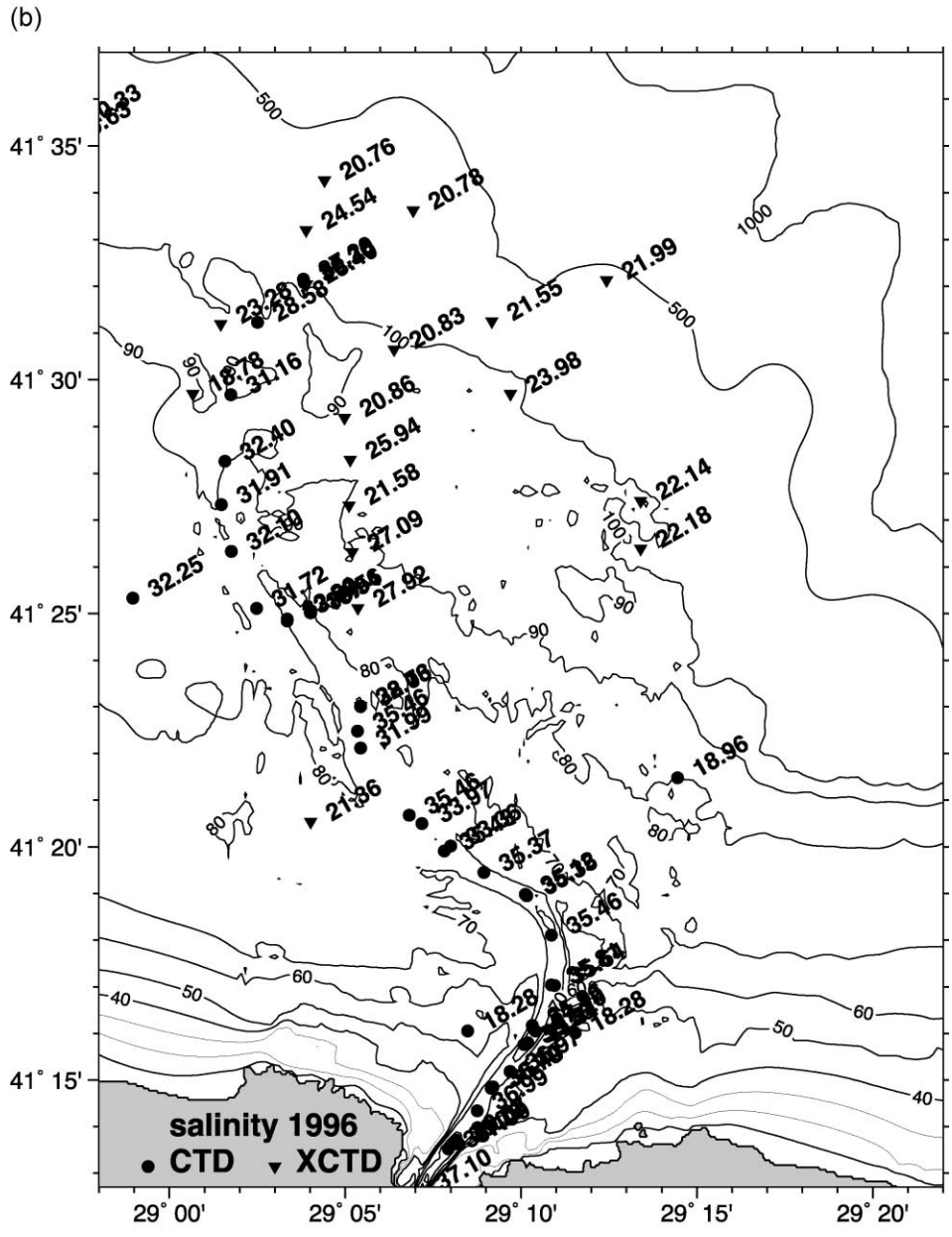

Fig. 6 (*continued*).

otherwise known to have mild bottom slopes is shown to have various submerged channels with a delta-like morphology and numerous terraces separated by discontinuities, which could be associated with small-scale faulting (Gökaşan et al., 1999). Although confined to a layer only a few meters in thickness, the water trapped in the depressions accumulated and overflowed across the terraces into ad-

joining regions, collecting along the west–east slope east of the main channel, destined finally to flow towards the deep Bosphorus Canyon.

4. Topography of the continental shelf

The bottom topography for the Black Sea shelf adjacent to the Bosphorus has been generated from a combined data set obtained from different sources: (i) digitized depth contours of UNESCO topographic maps for the Black Sea, (ii) digitized data from local hydrographic maps, (iii) ADCP depth measurements from R/V BİLİM cruise path in September 1994 with the combined data points shown in Fig. 8a, (iv) high-resolution topographical data (Fig. 8c) derived from the SWATH echosounder on board R/V ALLIANCE in 1995 (Di Iorio and Yüce, 1998) and 1996 (Di Iorio et al., 1999).

There were differences in the generated topography using different sources of data. The bottom topography generated when only (i–iii) depth data points of Fig. 8a were used is shown in Fig. 8b. The high-resolution topography (iv) obtained in the region surveyed with the SWATH system (Di Iorio et al., 1999) is shown in Fig. 8c, and the topography reconstructed by combining all the data from (i–iv) is shown in Fig. 8d. It is immediately clear that the

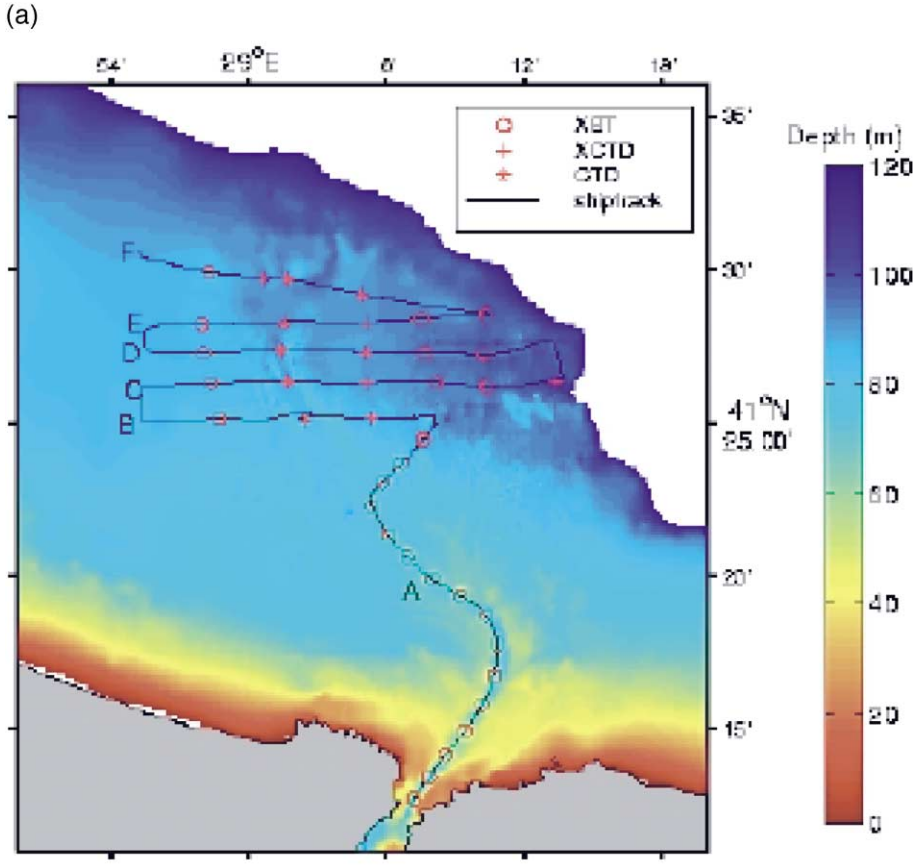

Fig. 7. (a) The ship track along transects made in the Bosphorus exit region in the Black Sea. The curved transect A leads northward from the Bosphorus across the shelf, while transects B, C, D, E and F are along the shelf. (b) High-resolution echo-sounding images along the west–east-oriented transects, together with overlaid temperature profiles from expendable sensors. Range is calculated along the path, starting from a point inside the Strait. (c) The same along the west–east-oriented transects with range calculated from the west end of each track. The darker areas correspond to higher values of relative acoustic backscatter intensity.

(b)

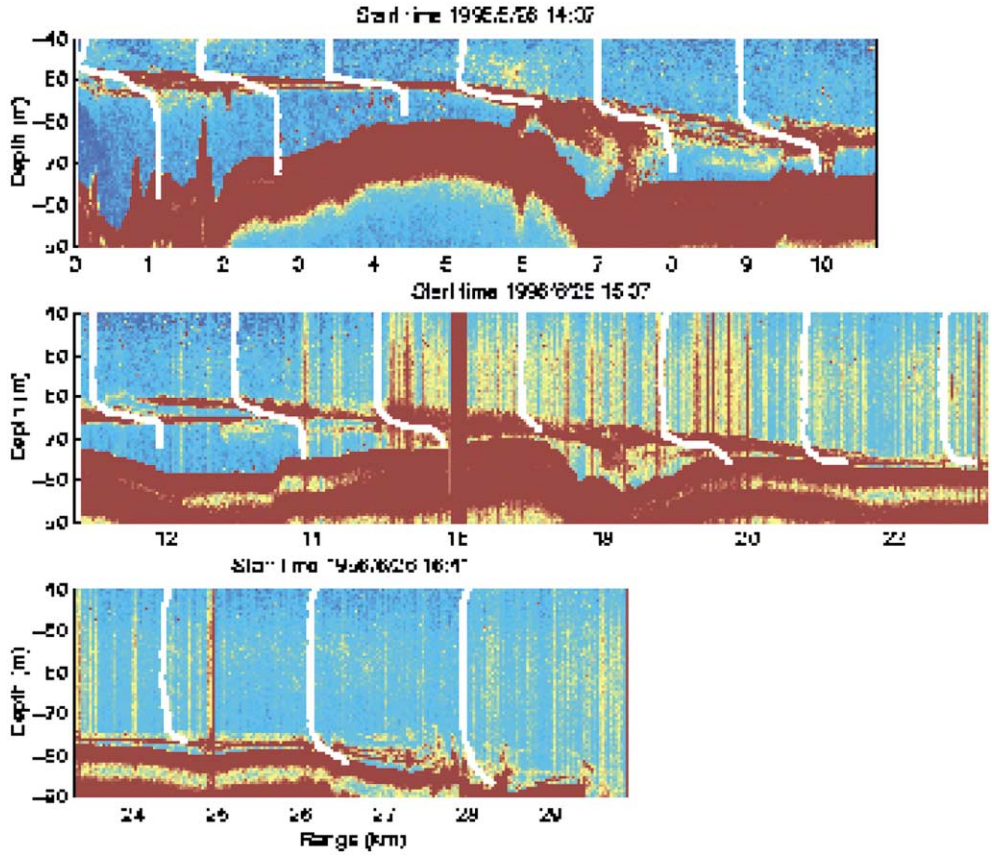

Fig. 7 (*continued*).

inclusion of SWATH data (iv) produces an abnormally deep area near the shelf edge not conforming to the information provided by other sources. This is demonstrated by correlating coinciding depth data from ADCP and SWATH measurements in Fig. 8e, which shows a positive bias in SWATH measurements yielding greater depths at the deeper areas that are inconsistent with the other sources of data, which had better consistency between themselves. This difference was important for modelling because the artificially high slopes near the shelf edge would tend to channel water towards the deep region. By combining the data from sources (i–iv) with the SWATH data corrected according to the regression in Fig. 8e, more consistent bottom topography was yielded as shown in Fig. 8f. The inclusion of the SWATH data also made a big difference near the Bosphorus exit, making the channel much wider and deeper compared to the case without these data as shown in Fig. 9a,b.

The detailed structure of the long groove leading up from the Bosphorus exit to the shelf edge is revealed for the first time, based on high-resolution digital data sets, although its structure had been visually observed earlier by analog echo sounding (Latif et al., 1991). The curved channel, its overflow ducts and the delta structure at the shelf edge are reminiscent of river morphology, which presently corresponds to the submerged salt-water outflow from the Bosphorus. It is not clear whether these features are in any way related to a hypothetical fresh-water stream that may have existed in the geological past.

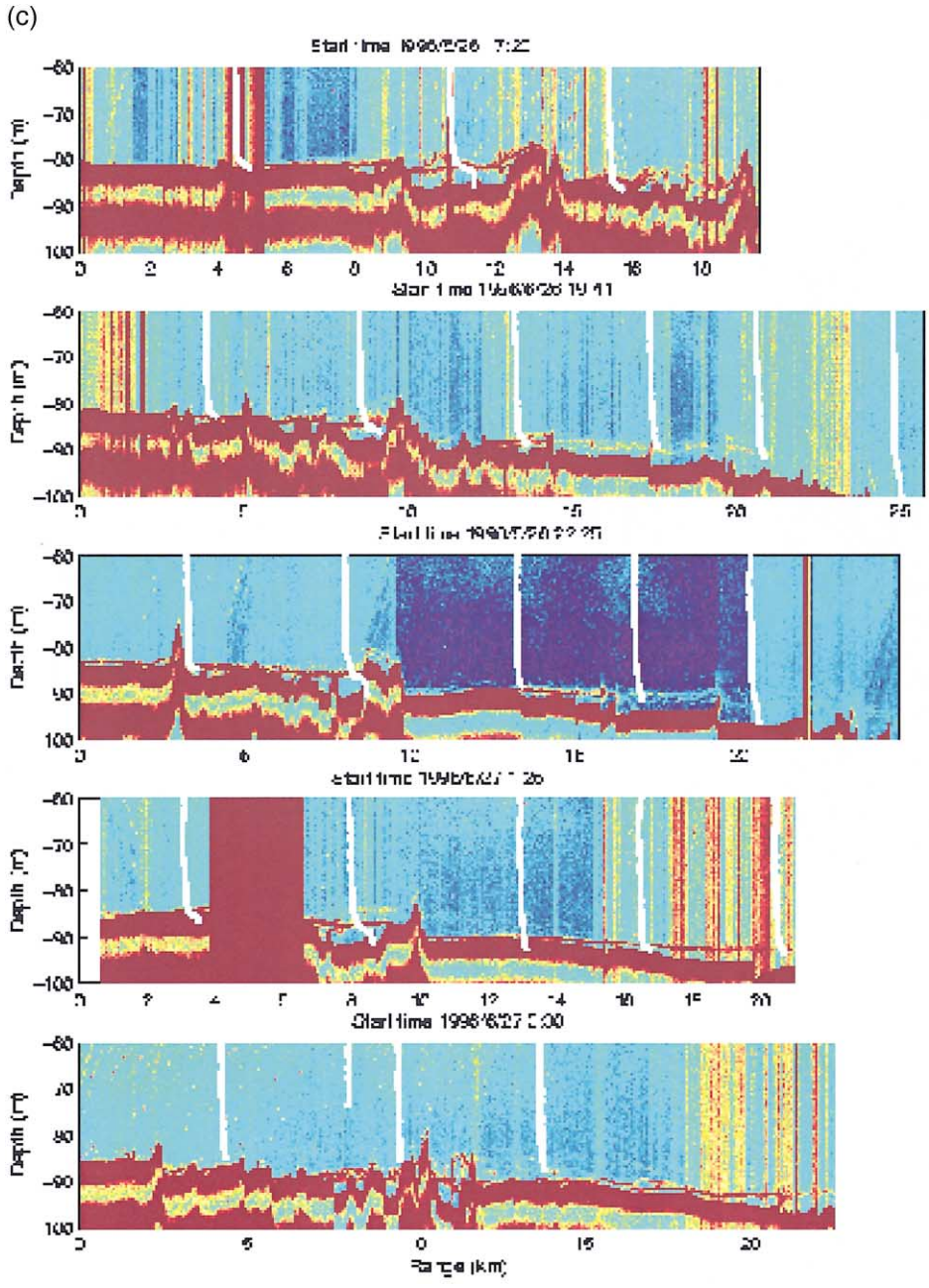

Fig. 7 (*continued*).

The deep canyon of the Bosphorus in the inner shelf area and the reformed bottom groove extending from mid-shelf to the shelf edge are continuously connected as shown in Figs. 6, 7a–c and 8f although this connection would not be clearly visible to most earlier observers if a special effort was not to be made. Incomplete observations could, thus, have incorrectly led to the speculation that 'no connection exists between the shelf-edge channels and the Bosphorus channel' (Demirbağ et al., 1999). Other

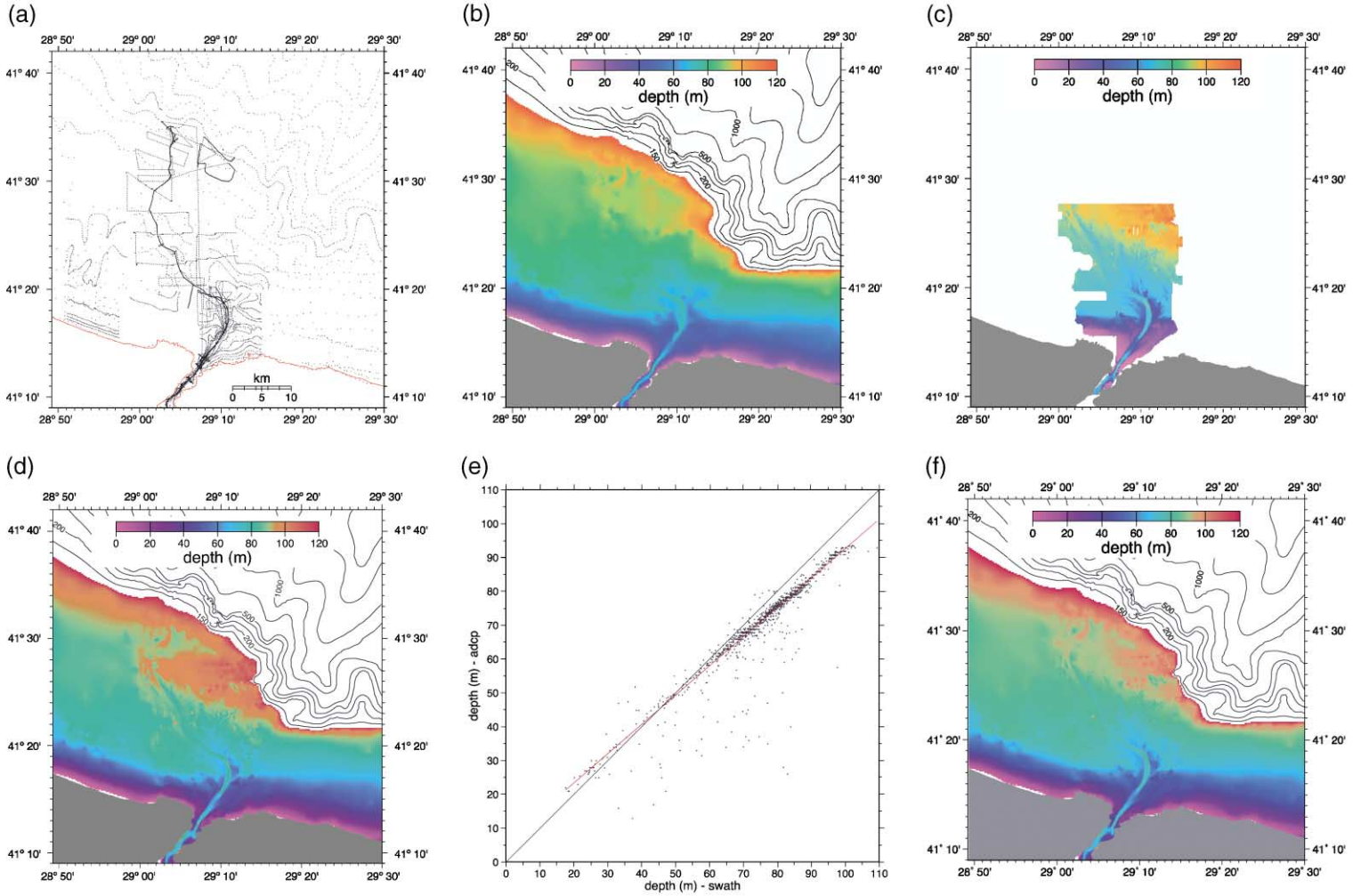

Fig. 8. (a) The geographic locations of depth points obtained from hydrographic maps and the 1994 ADCP depth measurements interpolated onto a model grid. (b) The resulting bottom topography. (c) The high-resolution bottom topography obtained from the combined data of the R/V ALLIANCE SWATH instrument in 1995 and 1996. (d) The resulting topography when combined with the other data. (e) The correlation of ADCP vs. SWATH depths at coinciding points. (f) The resulting topography when SWATH data are corrected according to the regression line.

interpretations based on incomplete sets of data have incorrectly attributed the cross-shelf channels to sand bars or waves formed by the rim currents of the Black Sea (Aksu et al., 1999).

5. Modelling of the shelf mixing and spreading of dense water

We use the Jungclaus and Backhaus (1994) model to study the Mediterranean plume in the Black Sea, incorporating the effects of the complex topography in the Bosphorus exit region. The model, described in Appendix A, is a reduced gravity single-layer approximation to the primitive equations (Jungclaus, 1994), including horizontal and bottom friction as well as entrainment from ambient waters. Either the Kochergin or the Pedersen entrainment parameterizations (Jungclaus and Backhaus, 1994) can be specified, taking into account the ambient property distributions, represented by realistic vertical profiles of temperature and salinity in the Black Sea.

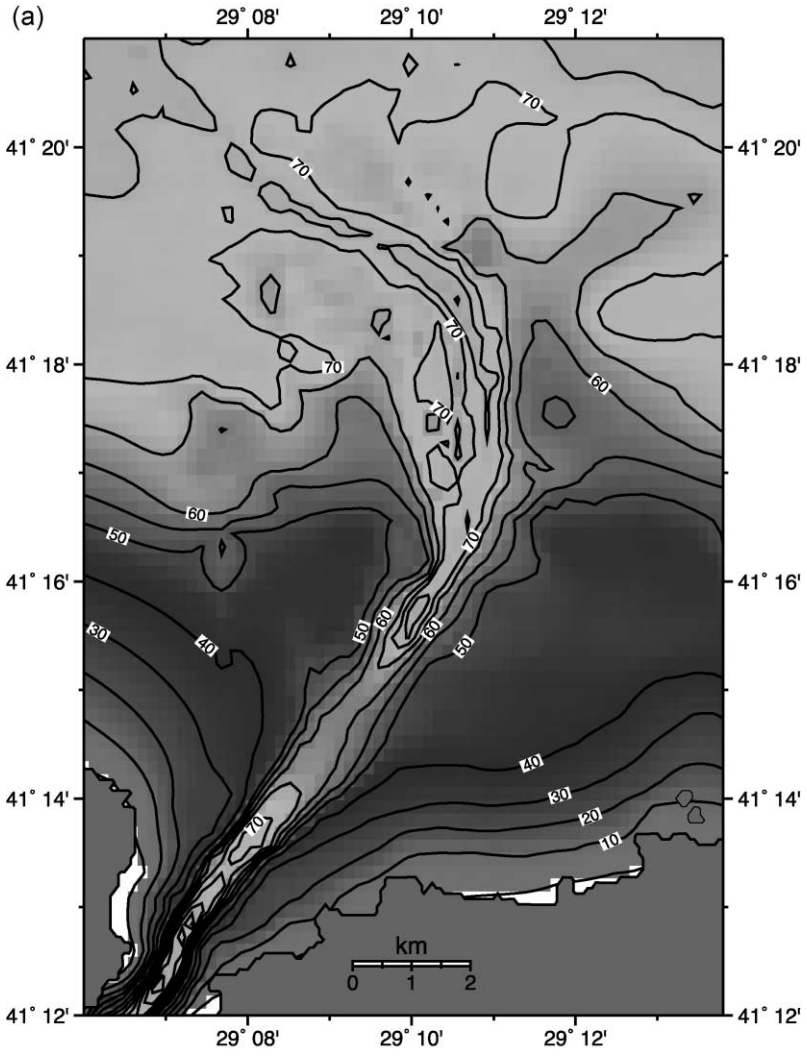

Fig. 9. Bottom topography of the Bosphorus exit region, displaying features the northern sill and canyon when the topography is constructed from (a) hydrographic maps and adcp depth soundings, and (b) when these data are combined with SWATH data.

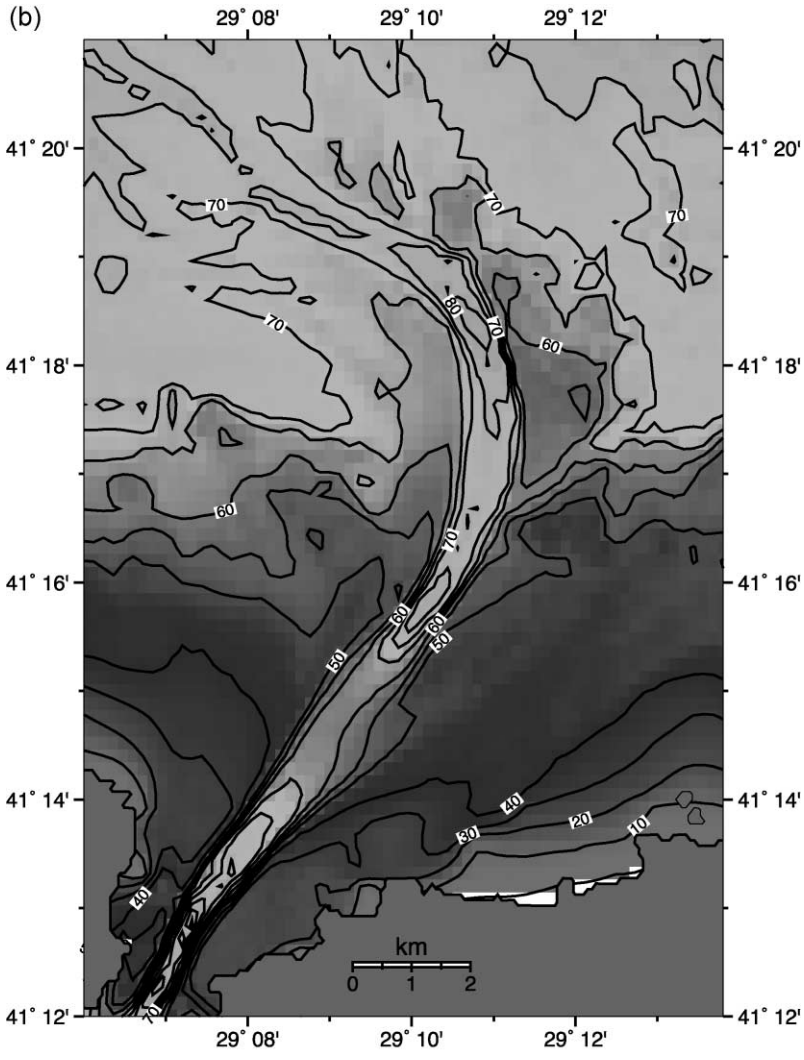

Fig. 9 (*continued*).

An order of magnitude analysis of the different terms in the momentum equations yields approximate balances between basic driving forces. We take basic scales of the motion, namely the length, velocity, total depth and layer depth as $L = 20$ km, $U = 0.5$ m/s, $D = 100$ m and $H = 5$ m, respectively, and the Coriolis parameter, f_o, at 41°N latitude. The relative importance of earth's rotation, measured by the ratio of Coriolis to inertial forces, i.e. the Rossby number, $R = f_0 L/U$, takes on a value of $R = 4$ with the above values. Similarly, the effects of bottom friction, measured by the ratio of friction to inertial forces take on values in the range $rL/D = 0.2$–3, while the ratio of buoyancy to inertial forces, i.e. the inverse Froude number, is $1/F^2 = g(\Delta\rho/\rho_0)H/U^2 = 1$. It is, therefore, clear that the flow of the Mediterranean water on the Black Sea shelf is the result of a first order balance between Coriolis, friction and buoyancy forces, as also revealed by theoretical considerations for such a flow (e.g. Shapiro and Hill, 1997; Shapiro and Zatsepin, 1997; Lane-Serff and Baines, 1998). Momentum transfer by lateral diffusion, characterized by the Ekman number, E, is much smaller, $1/E^2 = A_m/UL =$

0.075, and, therefore, the model results are not sensitively dependent on lateral friction.

In the present runs of the model, the ambient stratification was specified to be the observed profiles of temperature and salinity at station 7 of the 1988 R/V KNORR Leg 4 measurements (Özsoy et al., 1993). The horizontal resolution of the model is 200 m. The combined and corrected bathymetry data of Figs. 8f, 9b were used in the model. A central run of the model with indicated set of parameters and initial conditions is shown in Fig. 10 for day 10 after start up. After the first few days, the plume entirely covered the shelf where the flow apparently reached a steady state. Subsequent to these few days, a thick lense of water continued to develop and propagate east along the continental slope, owing to the Coriolis effect.

A comparison of the model results to measurements is made in the T–S diagram of Fig. 11. The average bottom-layer properties were calculated from profile measurements at stations presented earlier in Fig. 6. The plume properties obtained from the model at corresponding locations and the T–S relationship for the interior region have been superposed in the same figure. In general, the model results follow a straight-line relationship between the Bosphorus and ambient water characteristics representing direct, linear mixing between those sources, while the experimental data show much scatter as a result of complicated eddy mixing processes. There are various mechanisms not adequately accounted for by the model. Firstly, in reality, the plume is vertically stratified despite the sharp interface separating it from the ambient. The interfacial turbulent mixing in the model is parameterized by entrainment from a quiescent environment, while, in reality, active coastal flows and turbulence in the ambient waters could support local detrainment from, as well as entrainment into, the plume. The largest difference occurs especially in the region of the deep canyon adjoining the Bosphorus, where mixing in the model creates relatively more rapid dilution compared to the measurements indicating relatively more coherent property distribution. The differences between the model and observations get smaller in the wide shelf region approaching the shelf break. In 1994, the plume temperature and salinity differences between the measurements and the model results at all available stations were $\Delta T = 1.3 \pm 1.5$ (°C), $\Delta S = 1.8 \pm 0.9$; in 1996, they were $\Delta T = -0.7 \pm 1.2$ (°C), $\Delta S = -0.7 \pm 1.2$.

The discrepancy between the model and the observational data in Fig. 11 is expected in view of the simplifying assumptions used in model and the variety of other processes not accounted for at present. The model solution develops as a function of distance from the strait exit, and the discrepancy in early stages of plume development in the curved canyon region adjacent to the exit accumulatively affects the later results further offshore. Indeed, the difference between the model and observed data is largest at this initial reach and survives later in both simulations of Fig. 11a and b. In the initial region, the channel is very narrow, making it difficult to represent the flow with realistic velocity and entrainment using the present model resolution and lateral diffusion. These points are further discussed in the next section.

Entrainment is increased greatly at the steep continental slope and results in an order of magnitude increase in plume thickness in this region (Fig. 10b). In Fig. 12a, the depth dependence of the entrainment flux per unit depth shows that the flux peaks up at three different depth ranges: Firstly, near 50 m, at the depth of the interface over the sill, entrainment is increased as a result of the large flow velocities. The second peak occurs at around 70 m, at the average depth of the flat-shelf region, and the third peak occurs at around 110-m depth. The correspondence of the entrainment peaks to depth ranges is better displayed in Fig. 12b, presenting entrainment velocity distribution over the plume area. The large entrainment velocity near the sill corresponds to the first peak described above. The second peak at depth

Fig. 10. (a) Flow velocity, (b) layer thickness, (c) temperature and (d) salinity 10 days after the initialization of the model with continuous outflow from the Bosphorus. Run parameters are: $A_h = 150$ m^2/s, $r = 0.003$ for the horizontal eddy coefficient and bottom friction, respectively, and $u_o = 0.7$ (direction 45°) m/s, $S_o = 37$, $T_o = 14.5$ °C, $H_o = 40$ m for the initial conditions specified at the Black Sea exit of the Bosphorus. The velocity vectors are plotted at every 10 grid points to simplify the graphics. The thickness in the dark area along the continental slope is outside the scale range.

corresponds to middle depths of the flat shelf and, especially, to the region of easterly flow across the mild west–east slope towards Bosphorus canyon (see Fig. 10a,b), and the third peak corresponds to the cascade at the shelf break, where the steep continental slope forces an increase in entrainment.

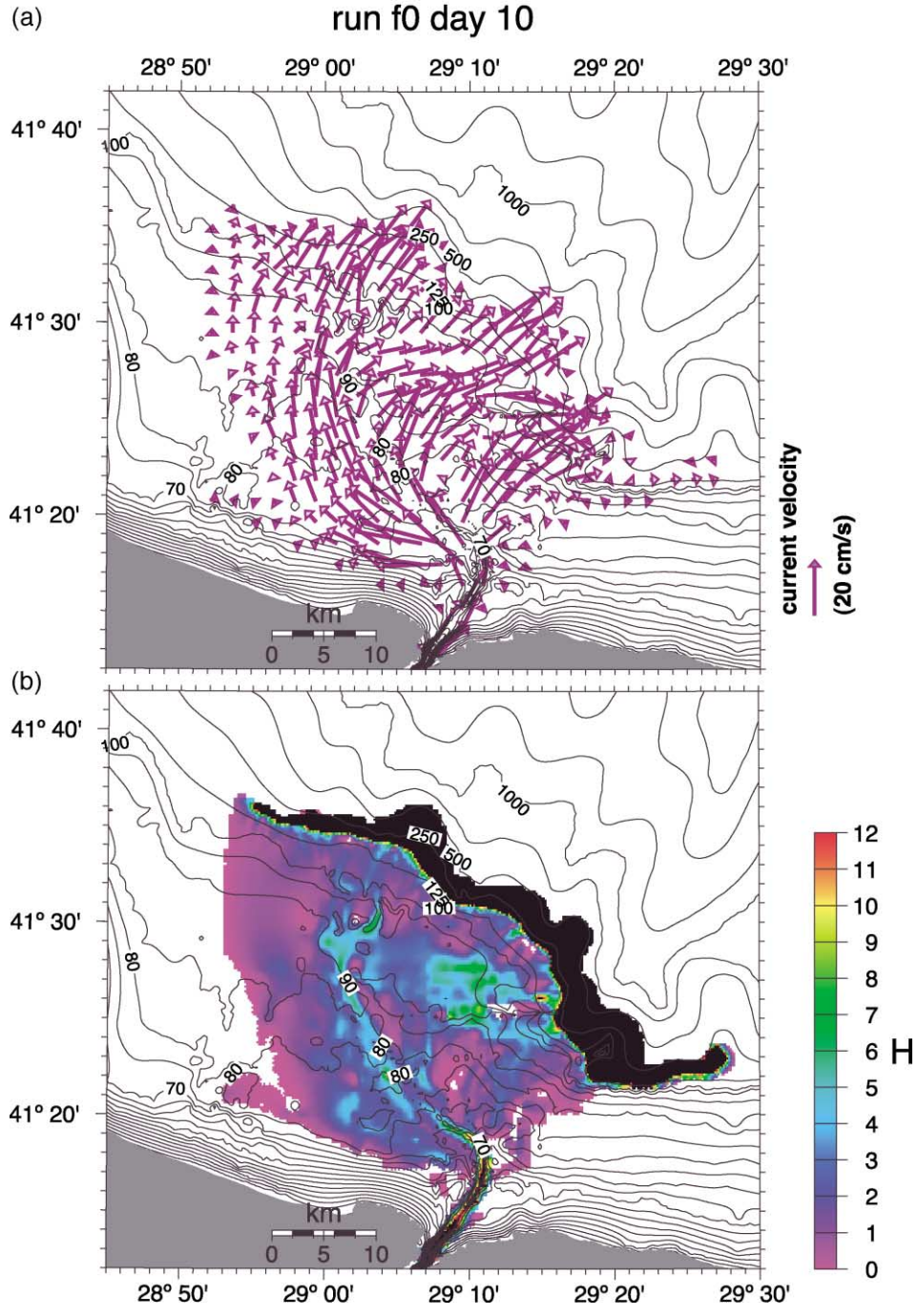

As the steep continental slope region and the wide shelf display significant differences in flow development, mean properties have been computed separately for the two regions. In Fig. 13, the top two panels display the entrainment flux and average salinity in the continental shelf and slope regions of

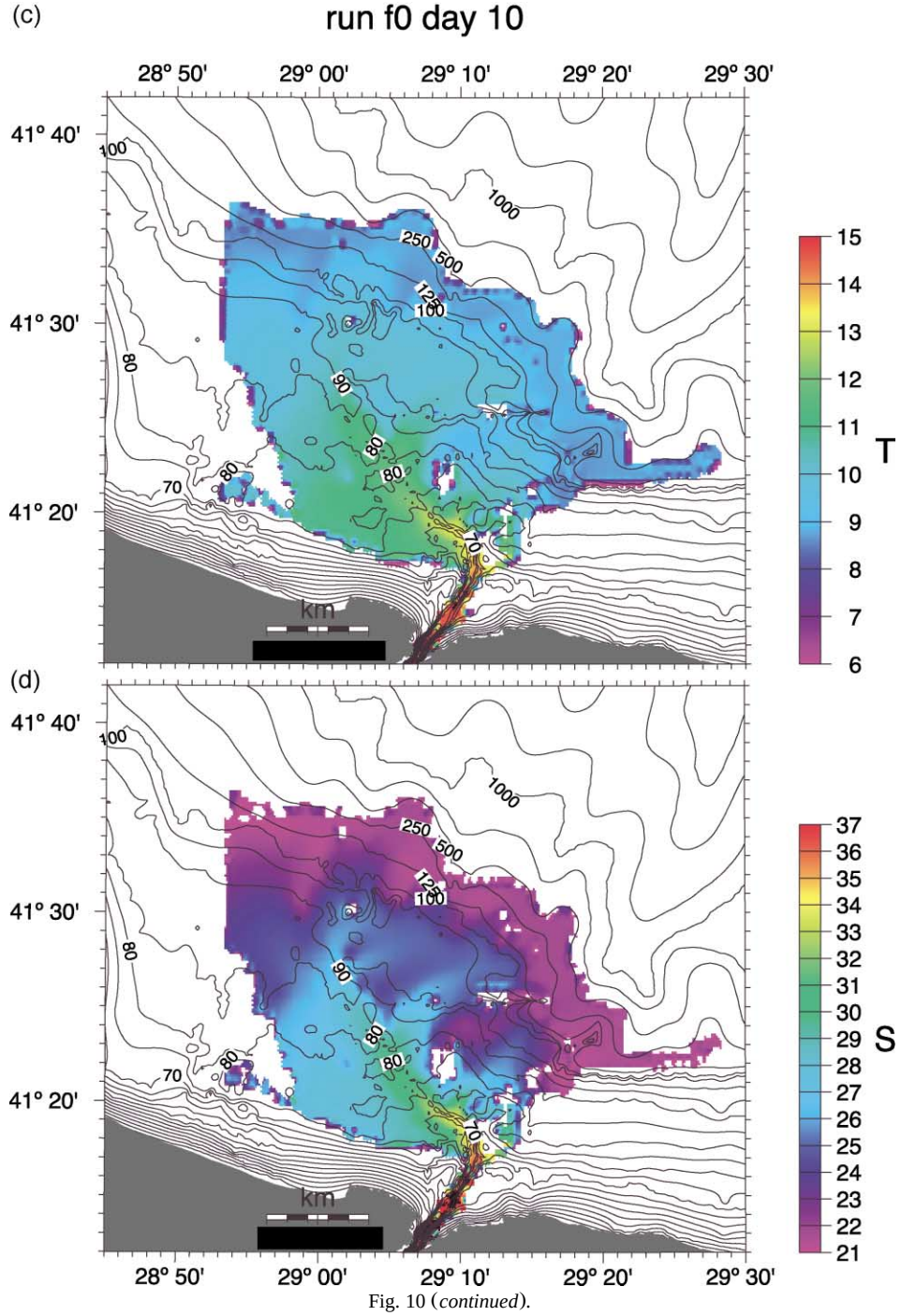

Fig. 10 (*continued*).

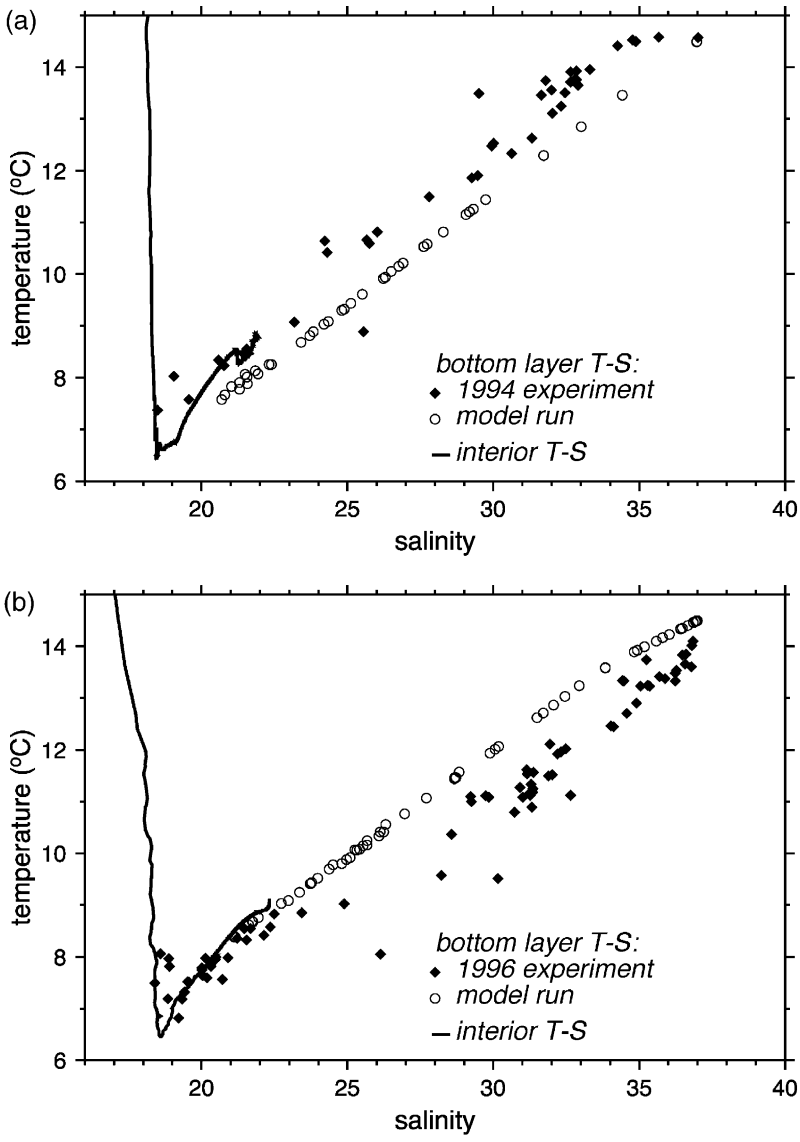

Fig. 11. Comparison of layer averaged temperature and salinity inside the plume based on model results and measurements for the (a) 1994 and (b) 1996 cases. The model results are obtained with parameters of Fig. 10 and correspond to ambient temperature and salinity profiles during each survey shown by the solid lines.

the plume separated by the 125-m-depth isoline, together with the ambient salinity averaged over the entire plume. It is observed that the shelf entrainment continues to increase until day 3, when the plume spreads and reaches the shelf edge, after which the entrainment flux at the slope region picks up, finally both reaching near steady state. The salinity in both regions reach stable values after about 3 days.

The last two panels of Fig. 13 show the average thickness and volume of the plume in the continental shelf and slope regions. The thickness of the plume stabilizes early on, day 1, or after about one inertial period, while its volume continues to increase by lateral spreading of until day 3, when it becomes constant as the plume reaches the shelf break in full width. The stable thickness of the shelf plume reached

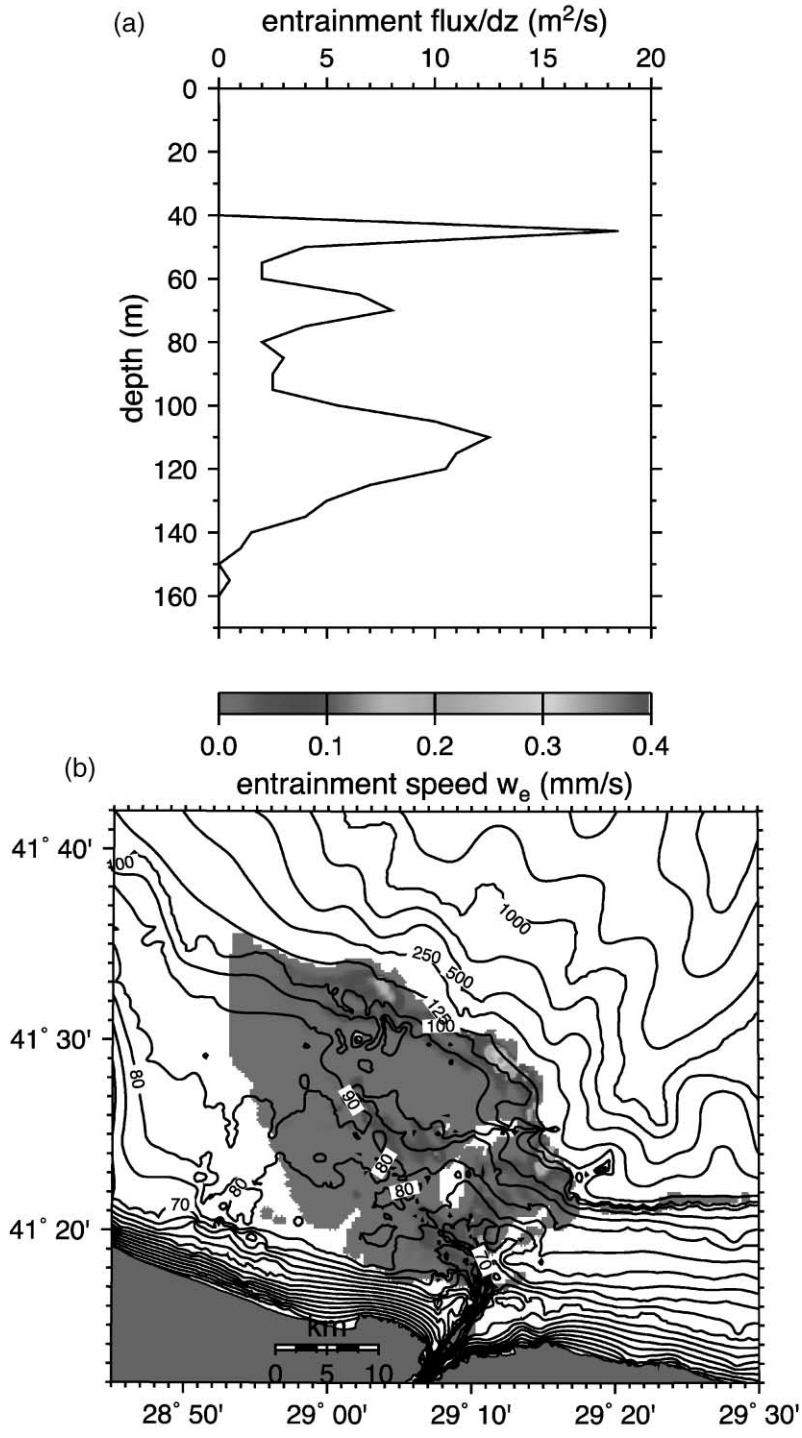

Fig. 12. (a) The depth dependence of the entrainment flux per unit depth, for the run conditions of 1994 experiment corresponding to Fig. 12a. (b) The horizontal distribution of the entrainment velocity, ω_e, for the same run.

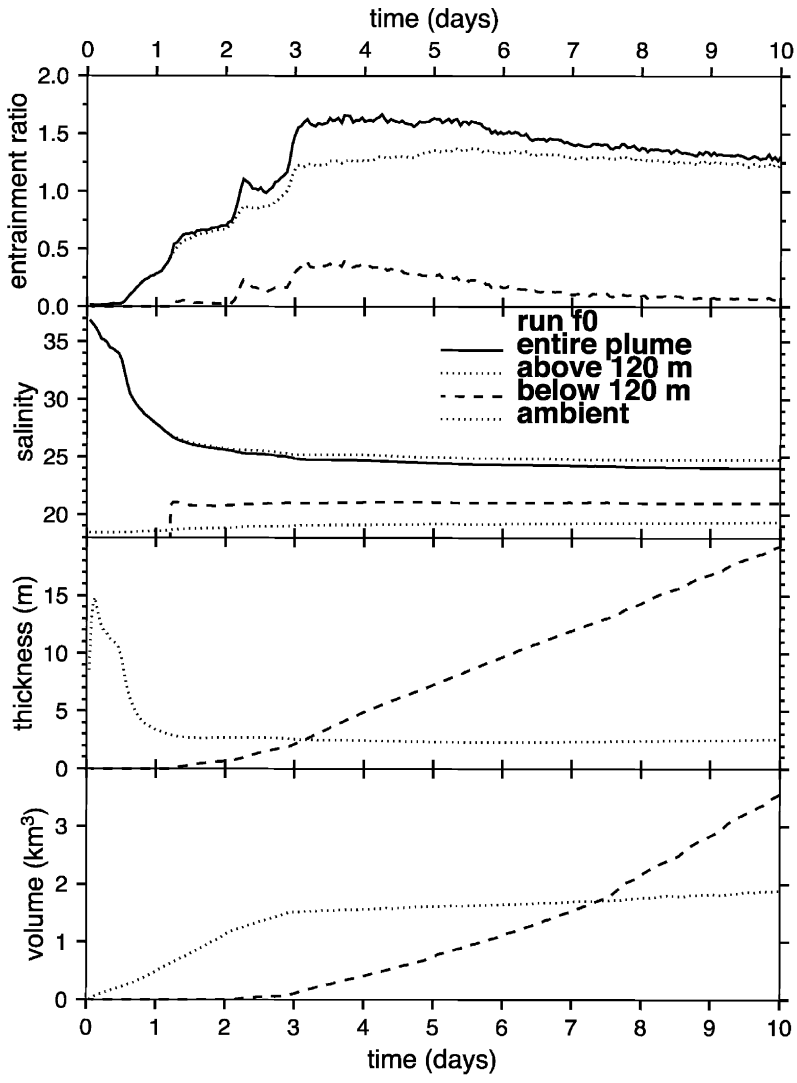

Fig. 13. The entrainment flux, average salinity, average thickness and average volume calculated for the plume on the continental shelf (depth < 120 m) and the continental slope (depth > 120 m) regions. The average ambient salinity for the area of the plume is also shown in the second panel.

almost after the first inertial period is in agreement with the predictions of Shapiro and Hill (1997), Shapiro and Zatsepin (1997) and Lane-Serff and Baines (1998), who scaled it with the characteristic Ekman layer thickness. On the other hand, the thickness and volume of the lense along the continental slope steadily rise as it swells with water supplied by entrainment and shelf outflow and progresses east along the continental slope.

There are certain limitations in regard to the interpretations based on the present model. Firstly, the density contrast of the plume is much reduced near the plume front, especially after the water cascades down the continental slope, where the assumption of a homogeneous layer is weakened and, hence, the reduced gravity approximation starts to fail. Furthermore, because the plume would have spent all of its density contrast and momentum near the level

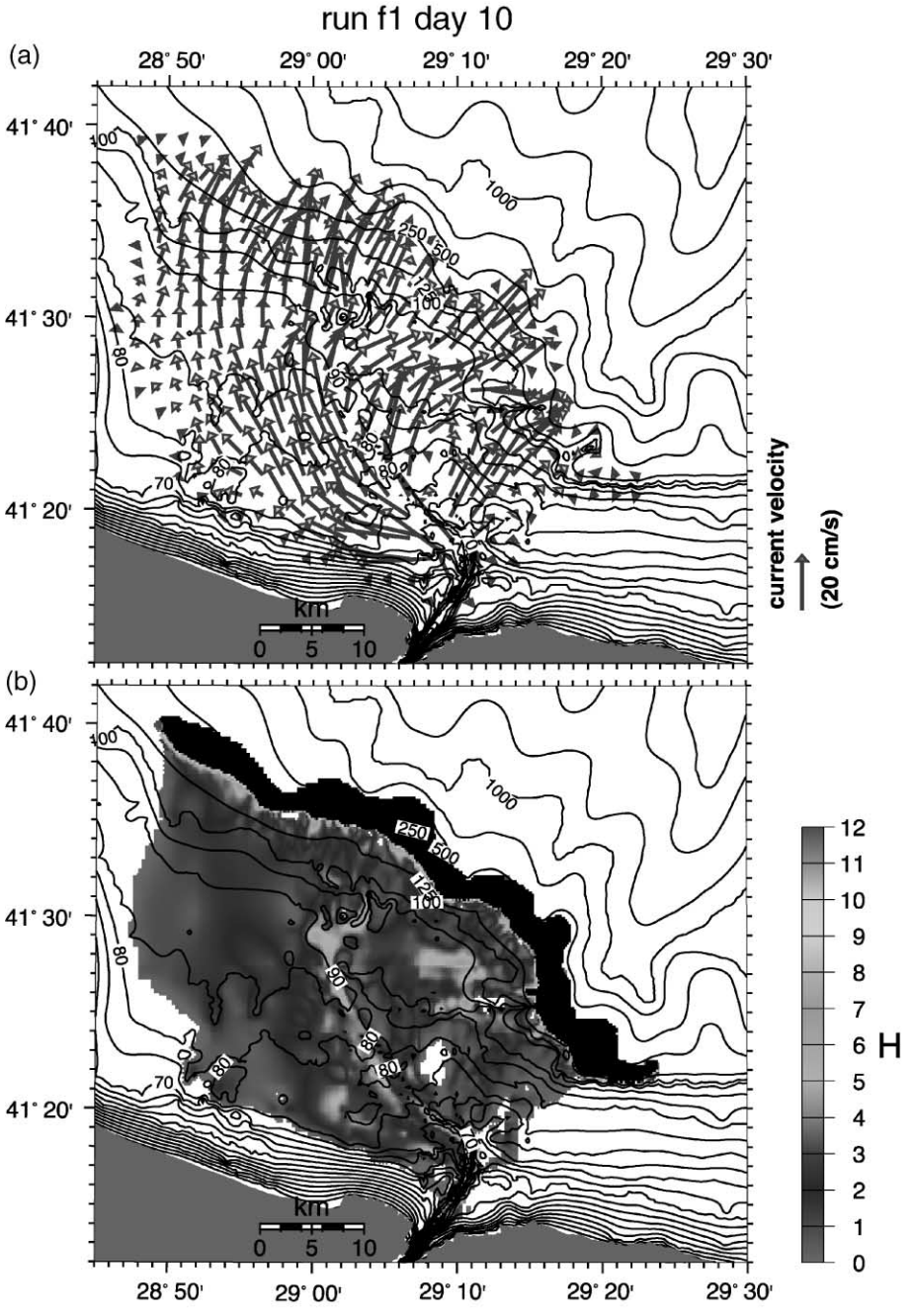

Fig. 14. Model results for (a) flow velocity and (b) layer thickness 10 days after initialization for the case when the efffects of earth's rotation has been inactivated by setting the Coriolis parameter to $f = 0$, while the other run parameters are the same as in Fig. 10, for (c) flow velocity and (d) layer thickness 10 days after start up for run parameters the same as in Fig. 10 except for the bottom friction $r = 0.015$.

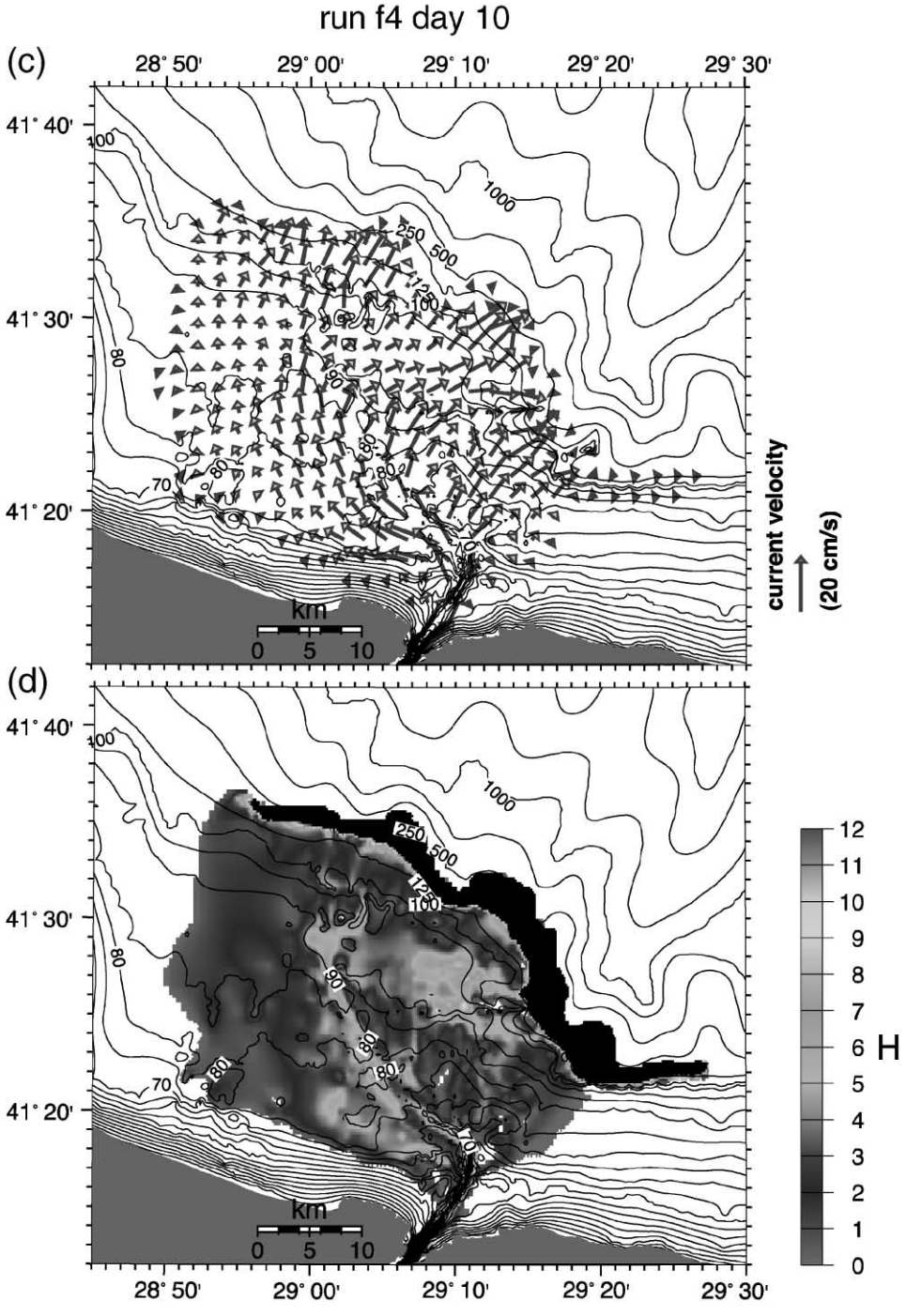

Fig. 14 (*continued*).

density equilibrium, it would tend to move east along bathymetric contours in the form of a lense while, at the same time, partly spreading into the interior by isopycnal spreading, which, however, is not treated by the present model, which only reproduces the easterly propagation of the lense.

6. Model sensitivity

The bottom drag coefficient, r, near the Black Sea exit of the Bosphorus was found to be in the range of 0.003 to 0.015 from acoustical measurements of flow and dissipation over the sill carried out in both 1995 and 1996 (Di Iorio and Yüce, 1998; Di Iorio et al., 1999). We have tested the model lower and upper bounds of this range in Figs. 10 and 14c,d to investigate its effects on the flow. Most literature references quote a value close to $r = 0.003$ for shallow seas (Jungclaus and Backhaus, 1994; Shapiro and Hill, 1997). Increasing the bottom friction coefficient from $r = 0.003$ in Fig. 10 to $r = 0.015$ results in smaller velocities in Fig. 14c,d, but does not greatly change the thickness or the salinity and temperature distribution (not shown). Decreasing the friction coefficient much further to $r = 0.001$ while increasing the initial velocity to $u_o = 1.0$ m/s at the same time in Fig. 15a,b results in increased velocities on the shelf as well as near the shelf edge, leading to the leakage of the dense water to the abyss at the continental slope. In the more relevant cases corresponding to higher friction values (Figs. 10 and 14c,d), the flow on the continental slope region has been trapped to depths shallower than 500 m, in agreement with the observations of Özsoy et al. (1993).

The other adjustable model parameter was the horizontal eddy coefficient ($A_m = 150$ m^2/s was used) though changing it had little impact on the results. Similarly, the use of linear vs. nonlinear model equations were of very little consequence for the simulated flow on the shelf. We also made runs setting the Coriolis parameter $f = 0$ to test the effects of earth's rotation on the flow. The plume properties do not change much between the central run and the nonrotational case in Fig. 14a,b, except that the plume in the nonrotating case was more spread out and thinner, whereas, in the rotational case, the flow was more confined and steered towards the east. The water at the plume front moved in both directions along bathymetric contours in the nonrotational case, while the motion along the bathymetric contours of the slope region was always to the east in the case with rotation.

Different formulations of entrainment, e.g. Kochergin vs. Pedersen formulations in Appendix A, had little effect on the results except for slight differences along the continental slope (not shown), not affecting the penetration depth of the plume. In the extreme case when entrainment was totally eliminated in Fig. 15c,d, a very thin layer of dense water conserving its initial properties flowed down the slope with great velocity, immediately reaching the abyssal depths.

The effects of ambient stratification were tested. However, changing the ambient stratification within reasonable limits, e.g. lowering the ambient profile by 30 m to simulate changes that would occur during a dynamically motivated change in the position of the pycnocline, was found to have only very little effect on the dilution and velocity distribution of the plume.

The model results were highly sensitive to topographic details, bottom friction and entrainment, and less to variations of the other parameters. The plume reached a quasi-steady state on the shelf area after about 10 days from startup. The flow along the continental slope is either in the form of a geostrophically adjusted motion along the bathymetric contours after it reaches a depth where it is arrested, or the precipitous flow down hill to abyssal depths, which continues to develop with time thereafter. The behaviour on the continental slope is rather erratic because the solutions reach limits of validity of the

Fig. 15. Model results for (a) flow velocity and (b) layer thickness 5 days after start up with run parameters the same as Fig. 10, except for reduced bottom friction $r = 0.001$ and increased initial velocity $u_o = 1.0$ m/s (direction 45°) specified at the Black Sea exit of the Bosphorus, (c) flow velocity and (d) layer thickness 10 days after start up, with run parameters the same as Fig. 10, but without entrainment.

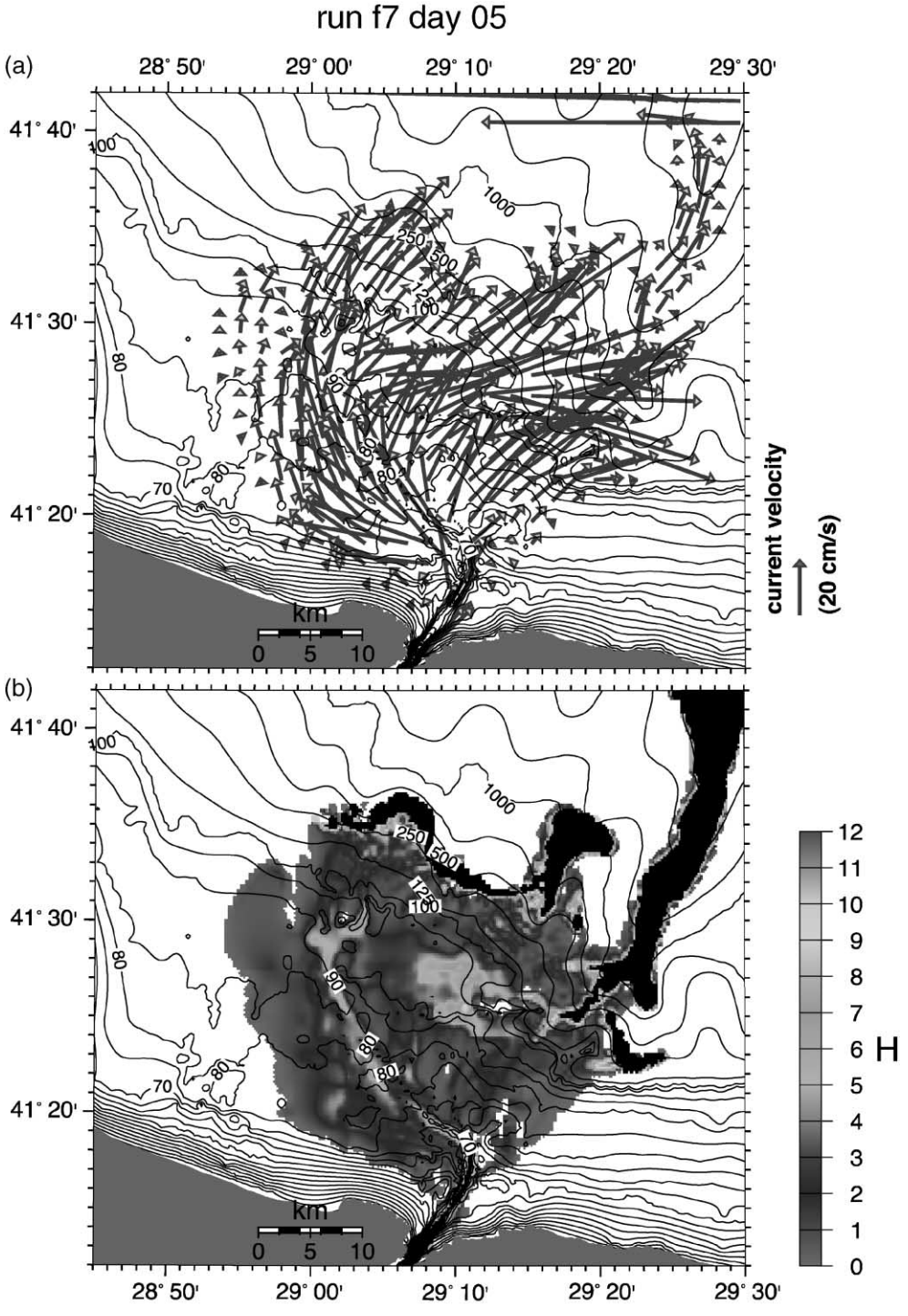
run f7 day 05
(a)
28° 50'
29° 00'
29° 10'
29° 20'
29° 30'
41° 40'
41° 30'
41° 20'
100
1000
250
500
125
100
80
90
80
80
70
80
km
0 5 10
current velocity
(20 cm/s)
(b)
41° 40'
41° 30'
41° 20'
100
1000
250
500
125
100
80
90
80
80
70
80
km
0 5 10
28° 50'
29° 00'
29° 10'
29° 20'
29° 30'
12
11
10
9
8
7
6
5
4
3
2
1
0
H

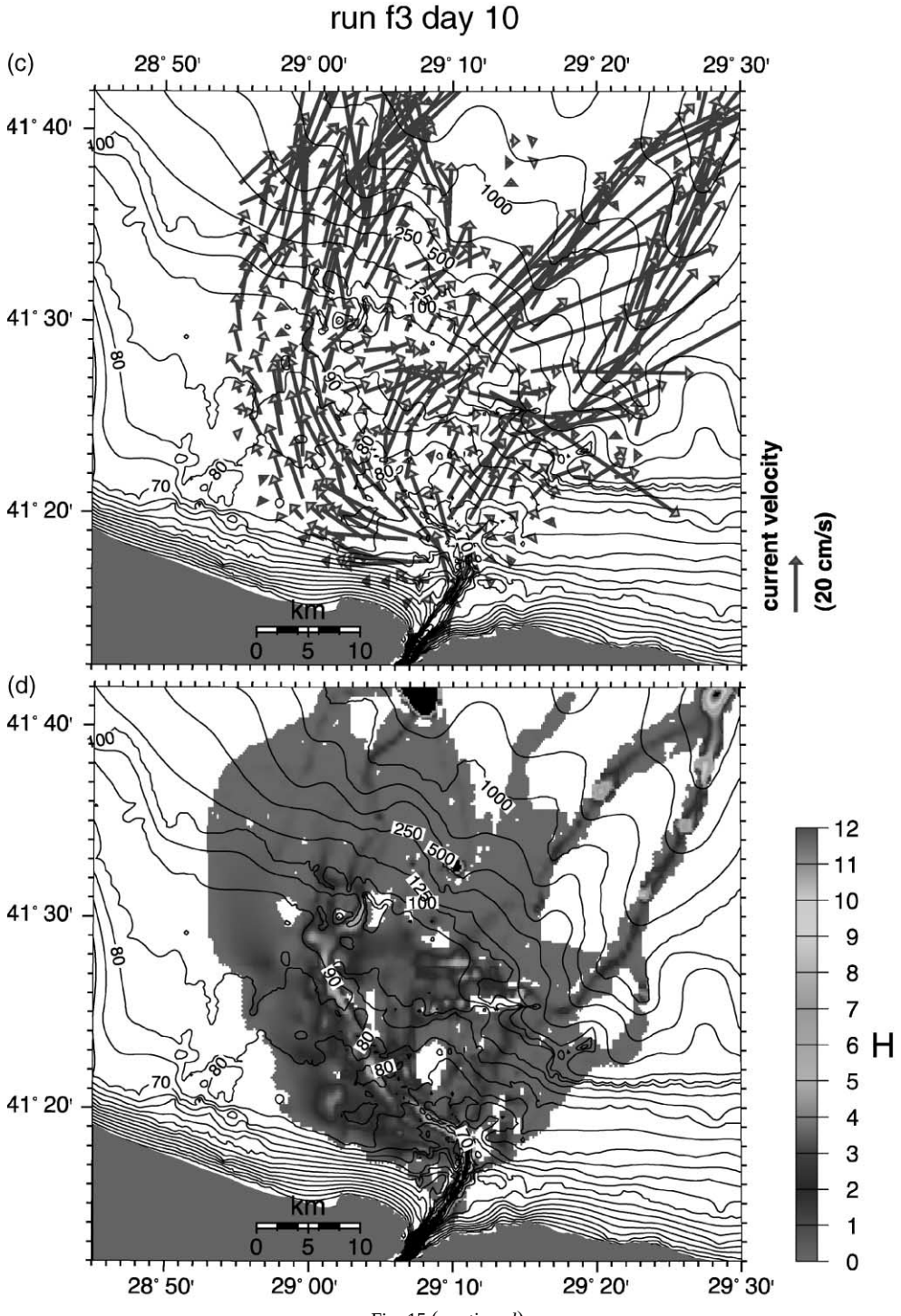

Fig. 15 (*continued*).

model itself: the rapid entrainment at the steep slope produces a very thick, diluted layer with vanishingly small density contrast at the edges of the plume. On the other hand, the assumptions with regard to entrainment are expected to break down in this steep region in relation to additional processes, such as due to double diffusive convection (Özsoy and Beşiktepe, 1995; Özsoy et al., 1993), and interaction with the numerous small-scale canyon features probably not adequately resolved in the present topography.

Seemingly small differences in bathymetry had relatively large impact on the spreading, mixing and, therefore, penetration of the Mediterranean effluent into the Black Sea. The sensitivity of the model to topography is explored in Figs. 16a–d and 17a–d, respectively, showing plume height and salinity for four different runs made with the parameters of Fig. 10, but with different topography.

To mention briefly, the model run with the topography of Fig. 8b with insufficient representation of fine-scale features (based on map and ADCP data alone) resulted in height and salinity fields in Figs. 16a and 17a, respectively. Compared to Fig. 8b, the flow in Fig. 16a is not appropriately channeled although the coverage and overall property distributions on the shelf are not too different from each other. The larger differences occur at the continental slope, with the cascading flow in the insufficiently resolved case (Fig. 16a) reaching depths of up to 1000 m within the Bosphorus Canyon, compared to a maximum depth of 500 m at the same time in the fine topography case (Fig. 8b). It can be observed that the improperly channelled flow escaping the bottom grooves then flows downslope to the east towards the Bosphorus Canyon before reaching the shelf further north, resulting in an accumulation of insufficiently diluted water at the canyon head, which then flows downslope to greater depth along the western flank of the Canyon.

With the inclusion of the uncorrected SWATH data (Fig. 8d), the topography was much improved near the sill and the curving canyon near the Bosphorus (Fig. 9b compared to a), therefore imposing less frictional and geometrical restraint to the flow in this region. As a result, the thickness of the plume in the curved canyon and shelf region increased in Fig. 16b although this thickening did not extend to the shelf-edge delta. The falsified eastward slope leading from the main channel towards the Bosphorus Canyon (Fig. 8d) resulted in leakage of the unrealistically thick layer of dense water towards the deep canyon (Figs. 16b and 17b). Because the dense water was transferred to the canyon slope with less dilution, it had greater depth penetration reaching depths of 1200 m as it proceeded along the eastern flank of the Bosphorus Canyon.

Two other runs were made to repeat the above cases with the same parameters and topography, but with a grid resolution of 600 m instead of the 200 m used earlier. The runs shown in the lower panels of Figs. 16 and 17 correspond to the runs in the upper panels repeated with the lower grid resolution. In both runs with imperfect topography and coarse resolution (Figs. 16c,d and 17c,d), the poorly sampled topography led to increased layer thickness, plume spreading and leakage of water outside the main channel. In both cases, the improper channelling of water resulted in greater dilution in salinity. The case with falsified shelf slopes and less restrained nearshore canyon features of the combined topography when it was coarsely sampled yielded much larger plume thickness and increased dilution everywhere in Figs. 16c and 17d. The penetration depth of the plume at the continental slope in both experiments were shallower than the corresponding cases with high-resolution cases, as a result of greater dilution before reaching the shelf edge.

Consistent results were only obtained when the corrected and combined high-resolution topography of Figs. 8 for Fig. 9b was utilized to yield the results in Figs. 10–13. Firstly, the plume thickness and salinity distribution was much improved to be sufficiently realistic in view of the observations. Secondly, the penetration of the shelf modified dense water reached only to a depth of 500 m, in agreement with modern observations.

It is perhaps worthy of note that the representation of the topography even in the best resolved case tested above could still be viewed as insufficient in some regards. Firstly, the scatter of depth data from two different sources in the correlogram of Fig. 8e and the numerous terraces, dykes and small-scale features revealed in Fig. 7c,d suggest infinitely more complex fine topographical features in the region. These small features can play a disproportionately large role in channelling or diverting the flow, or in

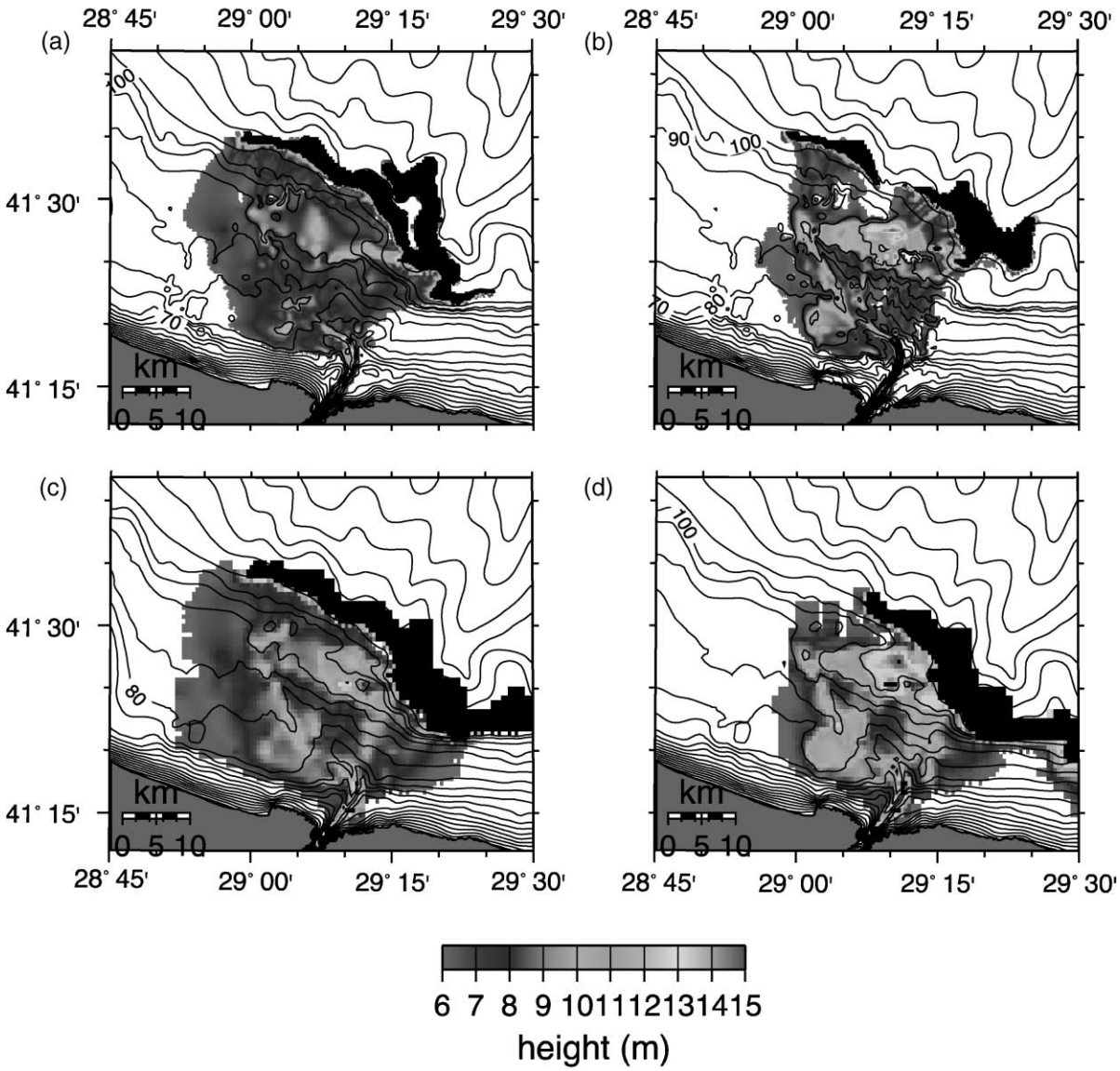

Fig. 16. Plume thickness obtained 10 days after startup with run parameters the same as Fig. 10, but for different cases of topographical representation: (a) simple topography of Fig. 8b and $\Delta x = \Delta y = 200$ m, (b) combined, but uncorrected topography of Fig. 8d and $\Delta x = \Delta y = 200$ m, (c) simple topography of Fig. 8b and $\Delta x = \Delta y = 600$ m, (d) combined, but uncorrected topography of Fig. 8d and $\Delta x = \Delta y = 600$ m.

exerting an effect of heterogenous mixing and friction, not adequately represented in the model even in the highly resolved model runs with homogeneous parameters. Despite the relative success of the model with the present improved representation of topography, there may still be room for further improvement.

Further effects anticipated in nature and not accounted for in the model determine the observed discrepancies between the modelled and observed behaviour of the Mediterranean dense water outflow. Firstly, a single active layer with inactive ambience idealized in the model excludes three-dimensional effects. For example, the effects of ambient currents,

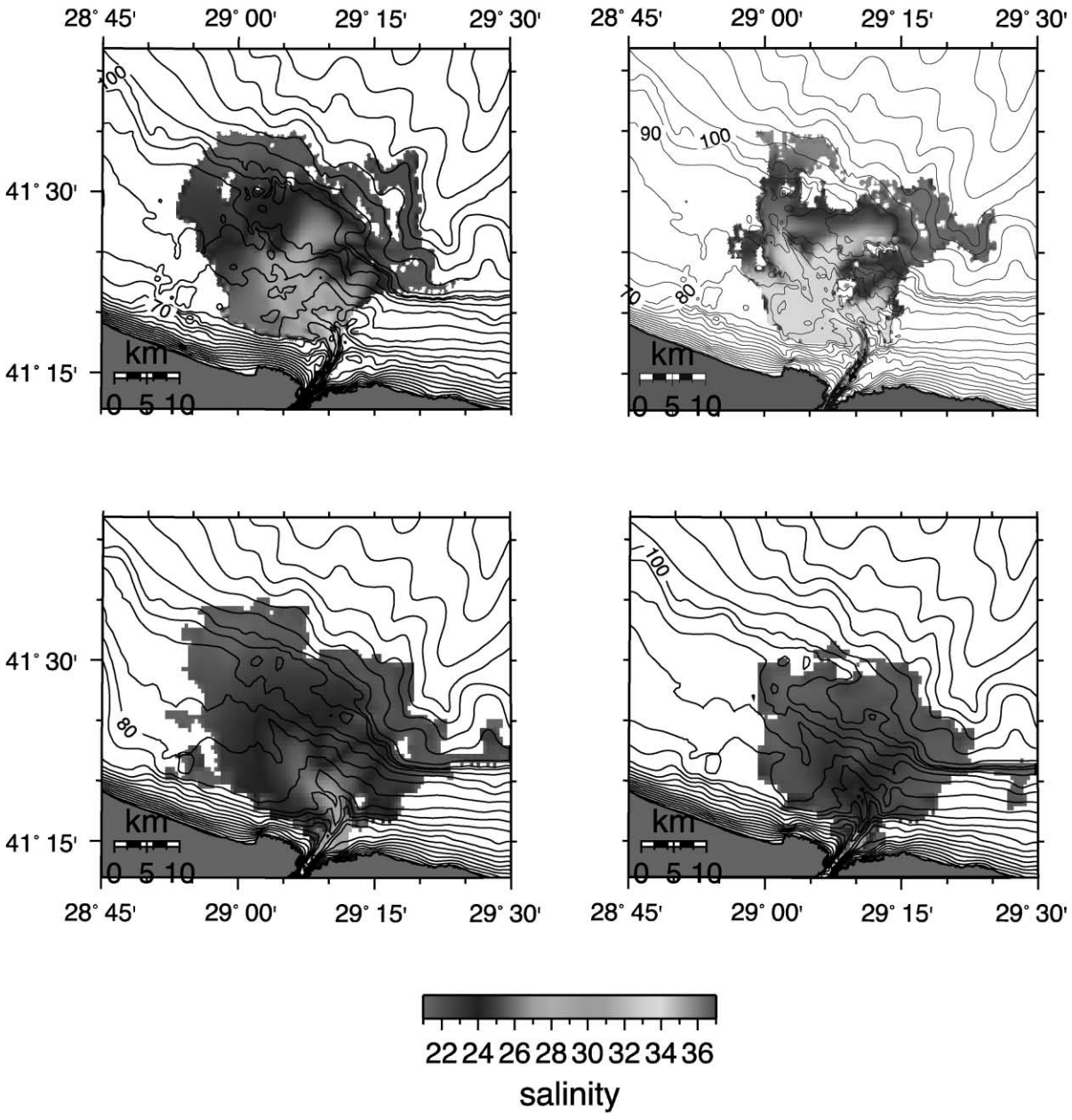

Fig. 17. Plume salinity obtained 10 days after startup with run parameters the same as Fig. 10, but for different cases of topographical representation: (a) simple topography of Fig. 8b and $\Delta x = \Delta y = 200$ m, (b) fine, but uncorrected topography of Fig. 8d and $\Delta x = \Delta y = 200$ m, (c) simple topography of Fig. 8b and $\Delta x = \Delta y = 600$ m, (d) fine, but uncorrected topography of Fig. 8d and $\Delta x = \Delta y = 600$ m.

e.g. the rim current of the Black Sea, possibly creating forced drainage of the plume (Shapiro and Hill, 1997), and instabilities in the flow (Shapiro and Zatsepin, 1997; Lane-Serff and Baines, 1998), the effects of viscous drainage from the lense and eddy formation in the upper layer (Lane-Serff and Baines,

1998), as well as isopycnal/double diffusive detrainment processes leading to the spreading of the arrested plume front from the continental slope into the interior, are features that are more difficult to handle, in general, and are not taken into account in the present model.

In a similar way, the effects of strait hydrodynamics are excluded from the present investigation although, in reality, these processes cannot be isolated from the dynamics of the exit region. Although strait dynamics is expected to influence the outflow, the working hypothesis for specifying boundary conditions in the exit region is derived from the existence of hydraulic control at the sill (i.e. a unique relationship between discharge and thickness of the lower layer). Although this particular requirement cannot be represented in the present model and although the establishment of the sill control depends on the other controls in the strait as much as it does on local flow characteristics, we are forced to isolate these effects by practical requirements. Unsteady effects are also unexplored for similar reasons. The forced simplification near the exit of the strait may be part of the reason for discrepancy between model and observed data in the initial region of the plume in Fig. 11a,b. Because the initial flow is not predicted with sufficient accuracy, it influences the local entrainment and has an accumulative effect on the further development of the plume.

7. Conclusions and discussion

Because the exchange and mixing at the Bosphorus have strong impacts in the adjacent seas and, in particular, in the Black Sea, it is important to obtain a sound understanding of these processes through the combined interpretation of observations and modelling. Continuing studies addressing the Bosphorus exchange and the ventilation of the Black Sea are important in their own right for clarifying the local effects of hydrometeorological and climatic changes, and have bearing on many applied problems, including the conservation of the Black Sea and the Marmara Sea and the safe regulation of navigation through the Strait, as the expected increases in the already heavy traffic threaten the well being of the population of one of world's largest cities and the health of the adjacent waters.

We have offered a glimpse of these processes in this brief account. However, the time-dependent regimes of exchange flows, mixing and entrainment in the Bosphorus and its Black Sea exit are possibly far more complex than described here. On the other hand, further analyses of the wealth of information obtained in the Bosphorus and the neigboring seas in recent years will certainly enhance the present understanding.

The 1994 measurements in the Bosphorus Strait have confirmed the well-known exchange properties although fine details of the change in water properties resulting from entrainment were revealed for the first time, based on high-resolution data. Identifying three distinct layers in the flow, the average salinity and thickness of the upper, lower and interfacial layers have been utilized to examine mixing effects. The most rapid changes are found to occur near the two principal control sections. Increased entrainment into either layer is found outside the region connecting these controls.

The combined results of measurements and modelling yield a better understanding of the Bosphorus outflow in the Black Sea. Firstly, the earlier results (Özsoy et al., 1998b) based on imperfect topography produced erratical behaviour of the plume with the flow speeding over an unrealistic shelf slope and resulting in unexpected deep penetration. With the refined topography, robust and representative results were obtained under a realistic range of parameters. The success of the model is demonstrated by reasonable agreement of its results with observed plume properties. The behaviour of the dense water outflow over the sill in the wide shelf and the steep continental slope regions differ considerably and have been described with respect to temperature, salinity, currents and entrainment characteristics.

Some features of the topography of the shelf adjacent to the Bosphorus is much like a river delta, providing a conduit for the Mediterranean water to reach the shelf without extensive mixing. However, at the same time, the details of this topography are important in determining the plume momentum and other physical properties at the shelf edge, before the Mediterranean water cascading down the slope loses much of its identity by rapid dilution through entrainment. Although the model starts to lose its validity on approaching this frontal region, the be-

haviour of the plume is only stable when the details of the bottom topography are well resolved, and the model predicts maximum penetration of the plume to depths of up to 500 m under the present ambient stratification, inflow conditions and a reasonable selection of the possible range of parameters.

The interpretation of newly discovered bottom features is beyond our present scope, but it can be expected to have an impact from a geological perspective. The bathymetric data reveal features of a possible drowned river channel with a bird-foot delta at the shelf edge. On the other hand, the relevance of this feature in geological terms is not so clear. A hypothesis of abrupt drowning of the Black Sea dated to about 7600 years BP has been based on the discovery of an erosion surface at a depth of ~ 105 m in the entire Black Sea, interpreted to represent the paleo-shoreline before the 'flood', and coinciding with the present outline of the shelf break (Ryan and Pitman, 1998; Ryan et al., 1998). The erosion surface is found to underlie the recent sediments (Aksu et al., 1999; Demirbağ et al., 1999) that the Bosphorus 'river channel' is found to cut through. While Ryan et al. (1998) link this erosion surface to abrupt flooding without specifying the exact mechanism, the interpretation of Demirbağ et al. (1999) suggest the breakthrough to have a tectonic basis. Indeed, the cross-sections in Fig. 7a–c as well as those given by Di Iorio and Yüce (1998) indicate previously undocumented terraces separated by sharp drops in depth, which could be part of the small-scale compressional faulting found in the Bosphorus region (Gökaşan et al., 1999) or, alternatively, could be related to steps of sea-level rise. Although the existence of a river in the region prior to flooding has often been suggested (Ryan and Pitman, 1998; Demirbağ et al., 1999), whether the Bosphorus outflow channel in its present form could in any way be linked to this 'hidden river' seems doubtful despite the fact that its delta at the shelf edge roughly coincides with the position and depth of the proposed ancient coastline.

Acknowledgements

This study has been made possible by combined opportunities to collect and analyze the relevant data, and to make use of modelling for a synthesis. A number of different projects were instrumental in this respect: The data used in this study were obtained on board the R/V BİLİM of the IMS-METU, during research programs supported by the Municipality of İstanbul, Water and Wastewater Administration (İSKİ), the Turkish Council for Scientific and Technological Research (TUBİTAK) as well as during a joint research activity of the IMS-METU and University of Washington scientists with additional support from the Office of Naval Research (ONR) of the United States, and during a research cruise on board the R/V ALLIANCE supported by NATO/SACLANTCEN with the participation of scientists from IMS-METU and the Department of Navigation, Hydrography and Oceanography (SHOD) of the Turkish Navy. Research grants from the NATO Science for Stability Program (ODBMS) Black Sea, the INCO-Copernicus Program of the European Union (ERBIC15CT960113) and TÜBİTAK (YDABÇAG 137) facilitated data collection, analyses and modelling. The authors wish to express their gratitude to the cooperative efforts of the scientists, technicians and graduate students of the cooperating institutions who took part in the data collection and processing, and the captains and crew of the ships who were involved in various stages of the work.

Appendix A

A.1. Model Description

The flow of the bottom layer of dense water is simulated by a hydrostatic, reduced gravity, two-dimensional primitive equation numerical model developed by (Jungclaus, 1994). The vertically integrated model predicts the spatial and temporal evolution of the flow field and the water mass changes within the gravity plume that descends on arbitrary topography. The turbulent lower-layer flow has height, H, within a total fluid height of D overtopped by the ambient upper layer of thickness $\zeta = D - H$ assumed to be at rest. Hydrostatic, vertically integrated primitive equations (between $z = -\zeta$ and $z = -D$) for the bottom layer are used together with the kinematic and dynamical boundary conditions at the limiting surfaces. The integrated transport of the

dense water is $\vec{\mathbf{U}} = (U, V) \equiv \int_{-D}^{\zeta} \vec{\mathbf{u}} \mathrm{d}z$, where $\vec{\mathbf{u}} = (u, v) \equiv \vec{\mathbf{U}}/H$ is the average velocity vector.

The continuity and momentum equations for the dense water layer are:

$$\frac{\partial \zeta}{\partial t} + \nabla \cdot \vec{\mathbf{U}} = \omega_{\mathrm{e}}, \tag{1}$$

$$\frac{\partial \vec{\mathbf{U}}}{\partial t} + \nabla \circ \left(\vec{\mathbf{u}} \cdot \vec{\mathbf{U}}\right) + f\hat{\mathbf{k}} \times \vec{\mathbf{U}} = -g'H\nabla\zeta - \frac{gH^2}{2\rho_{\mathrm{o}}}\nabla\rho + \nabla \cdot A_{\mathrm{m}} H \nabla \vec{\mathbf{u}} - \frac{\vec{\boldsymbol{\tau}}_{\mathrm{b}}}{\rho_{\mathrm{o}}}, \tag{2}$$

where the second term in Eq. (2) represents a dyadic operation, ω_{e} is an 'entrainment velocity', f is the Coriolis parameter, and $g' \equiv [(\rho - \rho_{\mathrm{a}})g/\rho_0]$ is the reduced gravity (in which ρ_{a} denotes the ambient and ρ_0 the reference density), A_{m} is the horizontal mixing coefficient for momentum and the bottom stress $\vec{\tau}_{\mathrm{b}}$ has a quadratic drag representation $\vec{\tau}_{\mathrm{b}} = \rho_0 r|\vec{\mathbf{u}}|\vec{\mathbf{u}}$.

The integrated conservation equations for heat and salt are in the following form:

$$\frac{\partial T}{\partial t} + \vec{\mathbf{u}} \cdot \nabla T + \omega_{\mathrm{e}} \frac{T - T_{\mathrm{a}}}{H} = \frac{A_{\mathrm{t}}}{H} \nabla \cdot (H \nabla T) \tag{3}$$

for temperature, and an equivalent form for salinity, coupled through the equation of state for seawater density $\rho = \rho\,(T, S, z)$ based on UNESCO (1981).

Entrainment occurs from the upper into the lower layer, with vertical speed, ω_{e}, pointed downwards and creates variations of plume scalar properties. Since the upper layer is assumed to be at rest, entrainment terms do not appear in the flux form of the momentum equation, but entrainment terms representing interfacial friction would emerge if the equation of motion were to be written in terms of velocity rather than transport. Turner (1973) parameterized the entrainment velocity as a function of the turbulent flow velocity, $\omega_{\mathrm{e}} = E|\vec{\mathbf{u}}|$, through a dimensionless entrainment coefficient, E.

Substantial work exists on turbulent entrainment (Turner, 1973; Pedersen, 1980), either in the case of a single turbulent layer entraining a nonturbulent fluid (Baringer, 1994; Jungclaus, 1994) or the case when both entraining layers are turbulent (Oğuz et al., 1990), all of which suggest that the entrainment velocity is a strong function of Richardson number:

$$Ri = \frac{N^2}{\left|\frac{\partial \vec{\mathbf{u}}}{\partial z}\right|^2} \qquad \text{where } N^2 = -\frac{g}{\rho_{\mathrm{o}}}\frac{\partial \rho}{\partial z}. \tag{4}$$

The Richardson number, Ri, measures the relative importance of the instability caused by shear with respect to the stabilizing in influence of density stratification (Turner, 1973). The Brunt-Vaisala (stratification) frequency, N, is a measure of static stability (Turner, 1973). When the stratification consists of two layers, with one of the layers in motion, we redefine:

$$Ri = \frac{g'H}{|\vec{\mathbf{u}}|^2} \text{ and } N^2 = -\frac{g\Delta\rho}{\rho_{\mathrm{o}} H}, \tag{5}$$

where H is the plume height and $\Delta\rho$ is the density difference between the layer and the ambience. Kullenberg (1977; cited in Jungclaus, 1994) equated the turbulent buoyancy flux to the flux arising due to entrainment at the interface:

$$k_{\mathrm{m}} \frac{\partial \rho}{\partial z} \equiv \omega_{\mathrm{e}} \Delta\rho, \tag{6}$$

where k_{m} represents the turbulent vertical exchange coefficient for density. Replacing the equivalent formulations for a single layer with uniform properties, therefore, yields:

$$\omega_{\mathrm{e}} = E|\vec{\mathbf{u}}| = \frac{k_{\mathrm{m}}}{H} = |\vec{\mathbf{u}}|\frac{c_{\mathrm{L}}^2}{S_{\mathrm{m}}}\sqrt{1 + \frac{Ri}{S_{\mathrm{m}}}}, \tag{7}$$

after using the formulation of Kochergin (1987, cited in Jungclaus, 1994) which gives the entrainment coefficient E as a function of Ri on the *rhs* of the above equation. Here, c_{L} is a constant of proportionality and S_{m} is the Schmidt number (the ratio of the momentum mixing coefficient, k_i, to the density mixing coefficient, k_{m})

$$S_{\mathrm{m}} = \frac{k_i}{k_{\mathrm{m}}} = \frac{Ri}{0.725\left(Ri + 0.186 - \sqrt{Ri^2 - 0.316\,Ri + 0.0346}\right)}. \tag{8}$$

Based on laboratory and field measurements, Pedersen (1980) alternatively found the dimensionless

entrainment parameter, E, to fit a theoretical function:

$$E = 0.072\left(\frac{r}{Ri}\right) \tag{9}$$

for values of $r/Ri < 10^{-2}$, where r is a dimensionless friction coefficient, typically having a value of $r = 0.003$.

The model utilizes both the Kochergin and Pedersen entrainment parameterizations as alternatives. Although Kochergin has derived $c_L = 0.05$, it is argued (Jungclaus and Backhaus, 1994) convincingly that the E vs. r/Ri curves for Kochergin and Pedersen entrainment parameterizations coincide for $r/Ri < 10^{-2}$ when the choices for constants are made as $c_L = 0.0275$ and $r = 0.003$. However, for higher Richardson numbers, the curve for Kochergin parameterization flattens, which, in fact, prevents unrealistically high entrainment rates at the shallow edges of the flow to be numerically calculated. We use $c_L = 0.0275$ in our calculations, but change r between 0.001 and 0.015.

A.2. The numerical scheme

The model discretization is made on the Arakawa staggered C grid, i.e. velocity is calculated at points displaced from the points where interface level (ζ), temperature and salinity are calculated. The points where the plume is absent are considered 'dry' (i.e. ζ equals total depth, D). The horizontal extent of the plume movable boundary is determined by the application of a Boolean logic sequence to test 'dry' or 'wet' points. Defining the plume elevations HE and HW at two neighboring pressure points (e.g. east and west of a velocity point, respectively), the point is set inactive if (i) both H_E and H_W points are dry, (ii) H_W point is dry and $\zeta_E > \zeta_W$, and (iii) H_E point is dry and $\zeta_W > \zeta_E$. In all other cases, the equation of motion is solved at the 'active' velocity point at each time step, Δt. For integration in time, the model uses an explicit scheme with two time levels is used for time integration, yielding plume height at $t + \Delta t$ and its extrapolation to $t + 2\Delta t$ so that negative plume heights are avoided at the edges of the flow, by introducing enhanced friction for the particular grid point to eliminate a consequence of numerical inaccuracies. Advection of momentum, as well as scalar properties (temperature and salinity), is done by using a conserving flux form of the equations, approximated by a selective (but numerically diffusive) vector upstream algorithm. The linear stability of the model is governed by:

$$\frac{\Delta x}{\Delta t} > \sqrt{g\frac{\Delta\rho}{\rho}\zeta}\,. \tag{10}$$

Reflections at the open boundaries of the model grid are handled via a numerical "sponge" zone, where the horizontal diffusion terms and grid spacing perpendicular to the open boundary are gradually increased.

References

Aksu, A.E., Hiscot, R., Yaşar, D., Mudie, P.J., 1999. Deglacial and postglacial water levels and water exchange across the Black Sea–Marmara Sea–Aegean Sea shelves, Eastern Mediterranean region. Land–Sea Link in Asia, International Workshop on Sediment Transport and Storage in Coastal Sea–Ocean System, Proceedings, pp. 463–468, Tsukuba, Japan, 485 pp.

Baringer, M.O., 1994. Mixing and dynamics of the Mediterranean outflow, PhD thesis, Woods Hole Oceanographic Institution/Massachusetts Institute of Technology Joint Program, Woods Hole, MA, USA.

Deacon, M.B. (Ed.), Scientists and the Sea 1650–1900—A Study of Marine Science. Academic Press, 445 pp.

Demirbağ, E., Gökaşan, E., Oktay, F., Şimşek, M., Yüce, H., 1999. The last sea level changes in the Black Sea: evidence from the seismic data. Mar. Geol. 157, 249–265.

Di Iorio, D., Yüce, H., 1998. Observations of Mediterranean flow into the Black Sea. J. Geophys. Res. 104, 3091–3108.

Di Iorio, D., Akal, T., Guerrini, P., Yüce, H., Gezgin, E., Özsoy, E., 1999. Oceanographic measurements of the West Black Sea: June 15 to July 1996, Saclant Undersea Research Centre report SR-305, 59 pp.

Ducet, N., Le Traon, P.-Y., Gauzelin, P., 1999. Response of the Black Sea mean level to atmospheric pressure and wind. J. Mar. Syst. 22, 311–327.

Etling, D., Gelhardt, F., Schrader, U., Brennecke, F., Khn, G., Chabert d'Hieres, G., Didelle, H., 2000. Experiments with density currents on a sloping bottom in a rotating fluid. Dyn. Atmos. Oceans 31, 139, 164.

Farmer, D.M., Armi, L., 1986. Maximal two-layer exchange over a sill and through the combination of a sill and contraction with barotropic flow. J. Fluid Mech. 164, 53–76.

Gökaşan, E., Demirbağ, E., Oktay, F.Y., Ecevitoğlu, B., Şimşek, M., Yüce, H., 1999. On the origin of the Bosphorus. Mar. Geol. 138, 183–199.

Gregg, M.C., 1998. Estimation and geography of diapycnal mixing in the stratified ocean. In: Imberger, J. (Ed.), Physical Processes in Lakes and Oceans. American Geophysical Union, Washington, DC, pp. 305–338.

Gregg, M.C., Özsoy, E., 1999. Mixing on the Black Sea shelf north of the Bosphorus. Geophys. Res. Lett. 26, 1869–1872.

Gregg, M.C., Özsoy, E., 2001. Flow, water mass changes and hydraulics in the Bosphorus. J. Geophys. Res., in press.

Gregg, M.C., Özsoy, E., Latif, M.A., 1999. Quasi-steady exchange flow in the Bosphorus. Geophys. Res. Lett. 26, 83–86.

Griffiths, R.W., 1986. Gravity currents in rotating systems. Annu. Rev. Fluid Mech. 18, 59–89.

Jungclaus, J.H., 1994. Ein numerisches modell zur simulation dichter Bodenströmungen im ozean mit anwendung auf den "overflow" durch die Dänemarkstraße, PhD thesis, Zentrum für Meeres-und Klimaforschung der Universität Hamburg Institut für Meereskunde, Hamburg, Germany.

Jungclaus, J.H., Backhaus, J.O., 1994. Application of a transient reduced gravity plume model to the Denmark Strait overflow. J. Geophys. Res. 99, 12375–12396.

Lane-Serff, G., Baines, P., 1998. Eddy formation by dense flows on slopes in a rotating fluid. J. Fluid Mech. 363, 229–252.

Latif, M.A., Özsoy, E., Oğuz, T., Ünlüata, Ü., 1991. Observations of the Mediterranean inflow into the Black Sea. Deep-Sea Res. 38 (Suppl. 2), S711–S723.

Marsigli, L.F., 1681. Osservazioni intorno al Bosforo Tracio overo Canale di Constantinopoli rappresentate in lettera all sacra real maesta di Cristina Regina di Svezia, Roma, 108+ pp.

Oğuz, T., Özsoy, E., Latif, M.A., Ünlüata, Ü., 1990. Modelling of hydraulically controlled exchange flow in the Bosphorus Strait. J. Phys. Oceanogr. 20, 945–965.

Özsoy, E., 1999. Sensitivity to global change in temperate Euro-Asian seas (the Mediterranean, Black Sea and Caspian Sea): a review. In: Malanotte-Rizzoli, P., Eremeev, V.N. (Eds.), The Eastern Mediterranean as a Laboratory Basin for the Assessment of Contrasting Ecosystems. NATO Sci. Ser. 2, Environmental Security, vol. 51. Kluwer Academic Publishing, Dordrecht, pp. 281–300.

Özsoy, E., Beşiktepe, Ş., 1995. Sources of double diffusive convection and impacts on mixing in the Black Sea. In: Brandt, A., Fernando, H.J.S. (Eds.), Double-Diffusive Convection. Am. Geophys. Union, Geophys. Monogr. vol. 94, pp. 261–274, 334 pp.

Özsoy, E., Ünlüata, Ü., 1997. Oceanography of the Black Sea: a review of some recent results. Earth Sci. Rev. 42, 231–272.

Özsoy, E., Ünlüata, Ü., 1998. The Black Sea. In: Robinson, A.R., Brink, K. (Eds.), The Sea: The Global Coastal Ocean: Regional Studies and Syntheses, vol. 11. Wiley, New York, pp. 889–914.

Özsoy, E., Ünlüata, Ü., Top, Z., 1993. The Mediterranean water evolution, material transport by double diffusive intrusions, and interior mixing in the Black Sea. Prog. Oceanogr. 31, 275–320.

Özsoy, E., Latif, M.A., Tuğrul, S., Ünlüata, Ü., 1995. Exchanges with the Mediterranean, fluxes and boundary mixing processes in the Black Sea. In: Briand, F. (Ed.), Mediterranean Tributary Seas, Bull. Inst. Oceanogr., Monaco, Special Number 15, CIESM Sci. Ser. No. 1, Monaco, pp. 1–25.

Özsoy, E., Latif, M.A., Beşiktepe, Ş., Gaines, A.F., 1995b. Fluorescent dye measurements of the mixing and transport of wastewater discharge in the Bosphorus. Water Sci. Technol. 32 (2), 61–68.

Özsoy, E., Latif, M.A., Sur, H.İ., Goryachkin, Y., 1996. A review of the exchange flow regimes and mixing in the Bosphorus Strait. In: Briand, F. (Ed.), Mediterranean Tributary Seas, Bull. Inst. Oceanogr., Monaco, Special Number 17, CIESM Sci. Ser. No. 2, Monaco, 1996.

Özsoy, E., Latif, M.A., Beşiktepe, Ş., Çetin, N., Gregg, N., Belokopytov, V., Goryachkin, Y., Diaconu, V., 1998. The Bosphorus Strait: exchange fluxes, currents and sea-level changes, In: Ivanov, L.I., Oğuz, T. (Eds.), Ecosystem Modeling as a Management Tool for the Black Sea, NATO Science Series 2: Environmental Security 47, Kluwer Academic Publishing, Dordrecht, vol. 1, 367 pp.+vol. 2, 385 pp.

Özsoy, E., Gregg, M., Föhrmann, H., Backhaus, J.O., 1998b. The Bosphorus Strait and its shelf outflow into the Black Sea: experiments and modelling. Oceanic Fronts and Related Phenomena, Proceedings of the Konstantin Fedorov International Memorial Symposium, St. Petersburg, International Oceanographic Commission Workshop Report No. 159, pp. 386–391.

Özsoy, E., Rank, D., Salihoğlu, İ., 2001. Pycnocline and deep vertical mixing in the Black Sea: stable isotope and transient tracer measurements. Estuarine, Coastal Shelf Sci., in press, EROS-2000 volume.

Pedersen, F.B., 1980. A monograph on turbulent entrainment and friction in two-layer stratified flow, Series Paper 25, Institute of Hydrodynamics and Hydraulic Engineering, Technical University of Denmark, Lyngby, Denmark.

Rank, D., Özsoy, E., Salihoğlu, İ., 1998. Oxygen ^{18}O, Deuterium and Tritium in the Black Sea and the Sea of Marmara. J. Environ. Radioact. 43, 231–245.

Ryan, W., Pitman, W., 1998. Noah's Flood. The New Scientific Discoveries About the Event that Changed History. Simon & Schuster, New York, 319 pp.

Ryan, W.B.F., Pitman, W.C., Major, C.O., Shimkus, K., Moskalenko, V., Jones, G.A., Dimitrov, P., Görür, N., Sakinç, M., Yüce, H., 1998. An abrupt drowning of the Black Sea shelf. Mar. Geol. 138, 119–126.

Shapiro, G.I., Hill, A., 1997. Dynamics of dense water cascades at the shelf edge. J. Phys. Oceanogr. 27, 2381–2394.

Shapiro, G.I., Zatsepin, A.G., 1997. Gravity current down a steeply inclined slope in a rotating fluid. Ann. Geophys. 15, 367–374.

Simeonov, J.A., Stanev, E.V., Backhaus, J.O., Jungclaus, J.H., Roussenov, V.M., 1997. Heat and salt intrusions in the pycnocline from sinking plumes; test case for the entrainment in the Black Sea. In: Özsoy, E., Mikaelyan, A. (Eds.), Sensitivity to Change: Black Sea, Baltic Sea and North Sea. NATO Sci. Ser. 2, Environmental Security, vol. 27. Kluwer Academic Publishing, Dordrecht, pp. 325–343.

Stanev, E.V., 1990. On the mechanisms of the Black Sea circulation. Earth Sci. Rev. 28, 285–319.

Stanev, E.V., Simeonov, J., Peneva, E., 2001. Ventilation of the Black Sea pycnocline by the Mediterranean plume. J. Mar. Sys. 31, 77–97 (this issue).

Staneva, J.V., Buesseler, K.O., Stanev, E.V., Livingston, H.D., 1999. The application of radiotracers to a study of Black Sea circulation: Validation of numerical simulations against observed weapon testing and Chernobyl ^{137}Cs data. J. Geophys. Res. 104, 11099–11114.

Sur, H.İ., Özsoy, E., Ünlüata, Ü., 1994. Boundary current instabilities, upwelling, shelf mixing and eutrophication processes in The Black Sea. Prog. Oceanogr. 33, 249–302.

Sur, H.İ., Ilyin, Y.P., Özsoy, E., Ünlüata, Ü., 1996. The impacts of continental shelf/deep water interactions in the Black Sea. J. Mar. Syst. 7, 293–320.

Turner, J.S., 1973. Buoyancy Effects in Fluids. Cambridge Univ. Press, London, 367 pp.

UNESCO, 1981. Tenth Report of the Joint Panel on Oceanographic Tables and Standards, UNESCO Technical Papers in Marine Science 36, UNESCO, Paris.

Ünlüata, Ü., Oğuz, T., Latif, M.A., Özsoy, E., 1990. On the physical oceanography of the Turkish Straits. In: Pratt, L.J. (Ed.), The Physical Oceanography of Sea Straits. NATO ASI Ser. Kluwer Academic Publishing, Dordrecht, pp. 25–60.

Wensink, H., Campbell, G., 1997. Bathymetric Map Production Using the ERS SAR. Backscatter 8 (1), 16–22.

Yüce, H., 1990. Investigation of the Mediterranean water in the Strait of Istanbul (Bosphorus) and the Black Sea. Oceanol. Acta 13, 177–186.

Zatsepin, A.G., Didkovski, V.L., Semenov, A.V., 1998. Self-oscillatory mechanism of inducing a vortex sloping bottom in a rotating fluid. Oceanology 38, 43–50.